

Nils Olav Jensløykken Meland

Infiltration of W-Cu composites

Developing a high-density material suitable for dampening systems

Master's thesis in Materials Science and Engineering

Supervisor: Ida Westermann

July 2020

Nils Olav Jensløyken Meland

Infiltration of W-Cu composites

Developing a high-density material suitable for dampening systems

Master's thesis in Materials Science and Engineering
Supervisor: Ida Westermann
July 2020

Norwegian University of Science and Technology
Faculty of Natural Sciences
Department of Materials Science and Engineering



Preface

This thesis is a part of specialization course TMT4905 Materials Technology, Master's Thesis at the Norwegian University for Science and Technology (NTNU) as part of the 5 years Master's Degree Programme in Materials Science and Engineering. Associate professor Ida Westermann of Department of Materials Science and Engineering has been the supervisor for the project. The project is in cooperation with Sandvik Teeness represented by Tormod Jensen and Einar Leo Ottesen as co-supervisors for the project. This master's thesis is a direct continuation of the project work conducted Fall 2019 [\[12\]](#), and both parts are a part of the research and development project NyDeMa at Sandvik Teeness.

Abstract

The aim of this thesis is to discuss whether the infiltrated product of W-Cu is a viable substitute for a damper mass component for the use in dampening systems. The mechanical properties were tested using tensile testing and were together with different microscopy techniques used to give an overview of the composite's performance compared with material specifications given for the application.

Sandvik Teeness develops and produces vibration dampening tools used for subtractive manufacturing. These tools are specialized for processes where it is necessary to machine over long overhangs. In these cases, vibration problems occur. The dampening system in these tools absorbs the vibrations, to ensure the machining processes yields clean surfaces.

Components used in dampening systems are made from a material of high density. Lead based materials need to be replaced due to environmental considerations. A substitute currently in use is based on a tungsten alloy made from a sintering process. The process yields high quality products but are expensive to produce. Therefore, an alternative material is proposed.

Three different samples, with two of the sample being W-Cu-Sn composites while the last sample is a W-Cu-Ni composite, were examined in this thesis. The samples were tested and compared with the material specification for the application. The W-Cu-Ni sample showed the largest elastic modulus 98.12 GPa, a large yield strength of 309.83 MPa and the largest total elongation 2.61% of the samples. The elastic modulus and total elongation criteria were not fulfilled for any of the samples, while the yield strength criterion was attained by all of them.

The conclusion is that W-Cu composites show good potential to be used for the given component for dampening systems. Some alterations to the material composition are needed to fulfil all the requirements along with improved infiltration, but the project is on the right path towards accomplishing the aim. The material fulfils the environmental considerations, and have the potential to be a viable substitute for the material for damper mass used in dampening systems.

Sammendrag

Formålet med denne masteroppgaven er å diskutere om det infiltrerte W-Cu produktet er en levedyktig erstatning for en dempermassekomponent for bruk i dempesystemer. De mekaniske egenskapene ble testet ved bruk av strekkprøving og var sammen med forskjellige mikroskopiteknikker brukt for å gi en oversikt over komposittens ytelse sammenlignet med materialspesifikasjoner gitt for applikasjonen.

Sandvik Teeness utvikler og produserer vibrasjonsdempende verktøy som brukes til drei- og fres operasjoner. Disse verktøyene er spesialiserte for prosesser der det er nødvendig å maskinere over lange overheng. I disse tilfellene oppstår vibrasjonsproblemer. Dempesystemet i disse verktøyene absorberer vibrasjonene, for å sikre at bearbeidingsprosessene gir fine overflater. Komponenter som brukes i dempesystemer er laget av et materiale med høy tetthet. Materialer basert på bly må byttes ut på grunn av miljøhensyn. En erstatning som for tiden er i bruk, er basert på en wolframlegering laget ved en sintringsprosess. Prosessen gir produkter av høy kvalitet, men er dyre å produsere. Derfor foreslås et alternativt materiale.

Tre forskjellige prøver, hvor to av prøvene var W-Cu-Sn-kompositter, mens den siste prøven er en W-Cu-Ni-kompositt, ble undersøkt i denne masteroppgaven. Prøvene ble testet og sammenlignet med materialspesifikasjonene for applikasjonen. W-Cu-Ni-prøven viste den største elastisitetsmodulen med 98,12 GPa, en stor flytespenning på 309,83 MPa og den største totale forlengelsen med 2,61% av prøvene. Elastisitetsmodul og den totale forlengelsen på prøvene nådde ikke de gitte kriteriene, mens flytespenningskriteriet ble oppnådd av alle tre. Konklusjonen er at W-Cu kompositter viser et godt potensial til bruk som materialet for den gitte komponenten for dempesystemer. Noen endringer i sammensetning er nødvendig for å oppfylle alle kravene i tillegg til forbedring tilknyttet infiltrasjonsprosessen, men prosjektet er på rett vei mot å oppnå målsetningen. Materialet oppfylder miljøhensynene og har potensial til å være en levedyktig erstatning for materialet brukt til dempermasse i dempesystemer.

Acknowledgement

I would like to acknowledge the Department of Materials Science and Engineering for supplying labs, equipment and supervision for using these. I would like to bring forward Chief Engineer Pål Christian Skaret for executing the tensile tests, Staff Engineer Berit Vinje Kramer for assistance and guidance with the metallographic grinding, polishing and other apparatus such as hardness tester and macroscope, and thirdly Senior Engineer Sergey Khromov for giving training with the SEM and EDS as well as been helpful with answering questions. I would also like to give a special thanks to Professor Ragnvald Mathiesen and Staff Engineer Ole Tore Buset at the Department of Physics, for conducting the CT scans.

I would also like to express my gratitude to Sandvik Teeness and the NyDeMa project group for funding the experimental work, for the exchange of knowledge and motivating me to perform, even during the troubling time during the covid-19 pandemic.

Abbreviations

Abbreviation	Explanation
APT	Ammonium Paratungstate
BCC	Body Centered Cubic cell
Bronze	Tin bronze
CT	Computerized Tomography
EBSD	Electron Backscatter Diffraction
EDS	Energy-Dispersive X-ray Spectroscopy
EHT	Electron High Tension
FCC	Face Centered Cubic cell
HV	Vickers hardness
IMP	Intermetallic phase
Ni 1	Test sample of infiltrated tungsten with copper & nickel powder
NTNU	Norwegian University of Science and Technology
OM	Optical Microscope
rpm	Revolutions per minute
Sandvik	Sandvik Teeness
SEM	Scanning Electron Microscope
Sn 2	Test sample of infiltrated tungsten with bronze powder 13-15 g/cm ³
Sn 13	Test sample of infiltrated tungsten with a bronze piece 11-13 g/cm ³
UTS	Ultimate Tensile Strength
W-Cu-Sn	Tungsten-bronze
WHA	Tungsten Heavy Alloys
YS	Yield Strength

Symbols

Symbol	Explanation
A_{tot}	Total elongation
d	Average diameter of pores in the tungsten
E	Elastic Modulus / Young's Modulus
e	Engineering strain
F	Force
G	Gravity coefficient
L_0	Initial gauge length
m	Mass
P_f	Internal friction force
P_s	Capillary force
q	Reduction of area
$R_{p0.2}$	Yield strength (0.002 strain offset)
s	Engineering stress
V	Volume with tensile test specimen
V_0	Initial volume
V_m	Volume fraction of matrix phase
V_p	Volume fraction of particulate phase
V_{tot}	Total volume
V_W	Volume fraction of tungsten in composite
C	Weight percentage
γ_L	Surface tension of molten copper
δ	Distance between adjacent linear peaks
ΔV	Change in volume
$\Delta\gamma$	Surface tension difference between two phases
ϵ	Energy conversion ratio
θ	Wetting angle between molten copper and solid tungsten
ρ	Density
ρ_c	Bulk density of composite
ρ_d	Relative density of composite
ρ_s	Theoretical density of composite

Contents

1	Introduction	1
1.1	Background and motivation	1
1.2	Aim and scope of the work	3
2	Theory	4
2.1	Tungsten-copper	4
2.1.1	Metal matrix materials	4
2.1.2	Forces during infiltration	5
2.1.3	Applications	7
2.2	Production of tungsten-copper	7
2.2.1	Mixing of powder	7
2.2.2	Press-sintering	7
2.2.3	Liquid phase sintering	8
2.2.4	Infiltration process	9
2.2.5	Water-cooling	9
2.3	Effects of alloying elements	10
2.3.1	Nickel, Cobalt and Iron	10
2.4	Rule-of-mixtures	11
2.5	Recycling	11
2.5.1	Raw tungsten resources	12
2.5.2	Overview of recycling methods	16
3	Experimental	23
3.1	Sample Preparation	24
3.2	Material properties	26
3.2.1	Density	26
3.2.2	Tensile Testing	27
3.2.3	Hardness	28
3.3	Microscopy	29
3.3.1	Macroscope	29
3.3.2	Computerized Tomography (CT)	30
3.3.3	Optical Microscope (OM)	30
3.3.4	Scanning Electron Microscope (SEM)	31
3.3.5	Energi-Dispersive X-ray Spectroscopy (EDS)	31
4	Results	32
4.1	Density	32
4.2	Tensile tests	34
4.3	Reduction of area (q)	37

4.4	Hardness	38
4.5	Macroscope	39
4.6	Computerized Tomography (CT)	43
4.7	Optical Microscope (OM)	44
4.7.1	Unaffected zone	44
4.7.2	Fracture area	47
4.8	Scanning Electron Microscope (SEM)	51
4.9	Energy-Dispersive X-ray Spectroscopy (EDS)	55
4.9.1	Point scan	55
4.9.2	Mapping	60
5	Discussion	64
5.1	Material properties	64
5.1.1	Density	64
5.1.2	Tensile tests	65
5.1.3	Reduction of area (q)	66
5.1.4	Elastic Modulus	66
5.1.5	Material specification	68
5.1.6	Hardness	69
5.1.7	Macroscope	70
5.2	Microstructure	70
5.2.1	CT	70
5.2.2	OM	71
5.2.3	SEM	72
5.2.4	EDS	73
5.3	Crucible material impact	74
5.4	Recycling and recovery	75
6	Conclusion	76
7	Further work	77
8	References	78
Appendix		81
A	Computerized Tomography (CT)	81

List of Figures

1	Cu-W binary phase diagram	5
2	Wetting angle during infiltration	6
3	Liquid phase sintering	8
4	Overview of production of W-Cu composites	10
5	W metal powder production route	13
6	Hydrochloric acid process	14
7	Solvent extraction process	14
8	Ion exchange process	15
9	Tungsten flow cycle	16
10	Overall recycling scheme	17
11	Overview of recycling from scraps	17
12	Zinc-melt process	18
13	Menstruum process	19
14	Cold stream process	20
15	Aqua regia leaching	21
16	Calcination followed by alkali leaching process	22
17	Infiltration setup	23
18	Fracture area analyses setup	25
19	Archimedes' law setup	27
20	Tensile test specimen specification	28
21	Macroscope setup	30
22	Density measurements by Archimedes' law	32
23	Tensile tests Sn 2	34
24	Tensile tests Sn 13	35
25	Tensile tests Ni 1	36
26	Tensile tests results	37
27	Reduction of area during tensile testing	38
28	Hardness	39
29	Macroscope Sn 2	40
30	Macroscope Sn 13	41
31	Macroscope Ni 1	42
31	Macroscope Ni 1	42
32	CT scan before tensile testing	43
33	CT scan of fracture area	44
34	OM Sn 2 - unaffected zone	45
35	OM Sn 13 - unaffected zone	46
36	OM Ni 1 - unaffected zone	47
37	OM Sn 2 - fracture area	48
38	OM Sn 2 - fracture area (high MAG)	49

39	OM Sn 13 - fracture area	50
40	OM Ni 1 - fracture area	51
41	SEM images - Sn 2	52
42	SEM images - Sn 13	53
43	SEM images - Ni 1	54
44	SEM Ni 1 - river pattern	55
45	EDS Point scan - Sn 2	56
45	EDS Point scan - Sn 2	56
45	EDS Point scan - Sn 2	57
46	EDS Point scan - Sn 13	57
46	EDS Point scan - Sn 13	58
46	EDS Point scan - Sn 13	58
47	EDS Point scan - Ni 1	59
47	EDS Point scan - Ni 1	59
47	EDS Point scan - Ni 1	60
48	EDS Mapping Sn 2	61
49	EDS Mapping of Sn 2 - elements	61
50	EDS Mapping Sn 13	62
51	EDS Mapping of Sn 13 - elements	62
52	EDS Mapping Ni 1	63
53	EDS Mapping of Ni 1 - elements	63
54	Tensile tests comparison	65
55	Elastic modulus vs composition	67
56	Theoretical density vs composition	68
57	SEM images comparison	72

List of Tables

1	Experimental data	24
2	Density calculations	33
3	Tensile properties	37

1 Introduction

1.1 Background and motivation

Sandvik Teeness develops and produces vibration dampening tools used for subtractive manufacturing in turning and milling operations for metalworking. The tools are specialized for processes where it is necessary to machine over long overhangs. In these cases, vibration problems occur. The dampening system in these tools absorbs the vibrations, to ensure the machining processes yields clean surfaces. These tools have a global market including industry for production of parts for aerospace and oil & gas components.

The component looked into in this master's thesis, is a damper mass made from a high-density material, with one alternative material composition for each of the density ranges 11-13 g/cm³ and 13-15 g/cm³ wanted. Materials currently in use needs to be changed either due to environmental considerations or due to high cost. The most common material used for this application is lead-based and need to be replaced due to the toxic nature of lead. A substitute currently in use is based on a tungsten alloy made from a sintering process. The process gives high quality products, but are expensive to produce. Therefore, an alternative material is proposed.

Tungsten-copper are metal matrix materials which have received much attention due to the combination of high conductivity and ductility from copper and low thermal expansion, high erosion resistance, high strength and high hardness from tungsten. For the given application high hardness, high erosion resistance and high strength in combination with ductility are the most important properties for the component. Conventional casting methods can not be used to produce the composite due to the huge gap between the melting points of the two elements. Powder metallurgy is then required.

[1, 10, 14]

There are two main routes to produce tungsten-copper composites, infiltration and liquid phase sintering. Due to the mutual insolubility of the two elements, composites with homogeneous microstructures and high density are difficult to fabricate. [22] Conventional sintering temperatures are ≥ 2000 °C. Infiltration temperature is commonly at 1250 °C, while liquid phase sintering temperature is around 1500 °C. As a result there is a large reduction in energy consumption with the use of infiltration compared to conventional sintering, and also compared to liquid phase sintering. [7, 14]

The industry is under constant development. As stronger and harder metals are needed, the subtractive manufacturing industry evenly needs stronger and harder materials for their components. Infiltration of tungsten-copper composites have the potential of much higher density, than what is used for the given application today. Tungsten-copper composites could therefore potentially be a viable material for many years to come.

The specialization project focused mainly on literature study to get a wider understanding of which methods are currently used for production of the composite. The focus of the literature study was on tungsten-copper composites, highlighting the subject of infiltration, while also taking liquid phase sintering and recycling into account. The literature study during the time span of the thesis further built upon the knowledge acquired during the specialization project. For the thesis the main focus were on the inclusion of nickel in the composite and the mechanical properties of tungsten-copper composites and other closely related tungsten heavy alloys (WHA).

The experimental work were focused around tensile tests manufactured from the different infiltration products fabricated at Sandvik, namely Sn 2, Sn 13 and Ni 1. The two former samples are W-Cu-Sn (tungsten-bronze) composites while the latter is a W-Cu-Ni composite. Mechanical properties were retrieved from tensile testing, microstructural features, fracture surface and composition analyses were also conducted, as well as testing the properties of hardness and density.

Theory regarding the tungsten extractive metallurgy and recycling were also included in the scope of the work by the request of Sandvik Teeness. On the path towards industrialisation, it is important to have a understanding of how to handle components at the end-of-life and how the elements can be recovered and/or recycled as part of a circular economy. Tungsten is a critical element [8] and therefore needs to be treated accordingly.

1.2 Aim and scope of the work

This thesis aims to look into tungsten-copper and relating alloys to find whether or not they are a viable substitute for the components currently in use for vibration dampening systems for turning and milling operations over long overhauls. The mechanical properties were compared to the material specifications given by Sandvik for the application. The specifications were namely; elastic modulus (E) above 190 GPa, yield strength (YS) above 200 MPa and elongation above 5%. The mechanical properties of the samples were expected to improve from the bronze samples Sn 2 and Sn 13 to the nickel sample Ni 1, because of the expected increase in sinterability and infiltration with the nickel inclusion.

The Ni 1 sample was expected to fulfill the material specifications and be deemed as a viable substitute for lead-based components. The microstructural and fracture surface examinations were anticipated to reveal possible improvements to the production and the theory will be used to propose measures to be taken to further promote the viability of W-Cu-Ni composites as a damper mass.

2 Theory

2.1 Tungsten-copper

Tungsten is a transition metal with the highest melting point of all discovered elements, melting at 3410 °C. Copper has a melting point of 1085 °C in comparison. Other notable properties of tungsten are high hardness, low thermal expansion coefficient, high strength and high resistance against wear and erosion. Compared to copper, tungsten has more than twice the density, with 19.25 g/cm³ at 20 °C (8.94 for copper). Tungsten exhibit body-centered cubic (BCC) crystal structure, while copper exhibit face-centered cubic (FCC) crystal structure. [4, 10, 14, 22]

2.1.1 Metal matrix materials

Metal matrix materials are composite materials combining properties from two different metals to inherit the greatest properties of each of them. In this way the material made have superior properties to fulfill various application, and are especially needed for heavy duty applications, where there are high requirements for combination of properties.

One of the key combination of properties are the combination of high strength and ductility. For most materials one property comes at the expense of the other. These are however possible to combine in metal matrix materials by using one strong and hard component along with a softer and more ductile one. This is the case for tungsten-copper composites.

The two components do not easily mix, with low mutual solubility as can be seen in the phase diagram in Fig. 1. The dissimilar melting points make the composites not possible to produce with conventional methods, such as casting. Therefore more complex methods needs to be applied. As a result the superior properties comes at a cost of the expensive manufacturing routes required to produce the material.

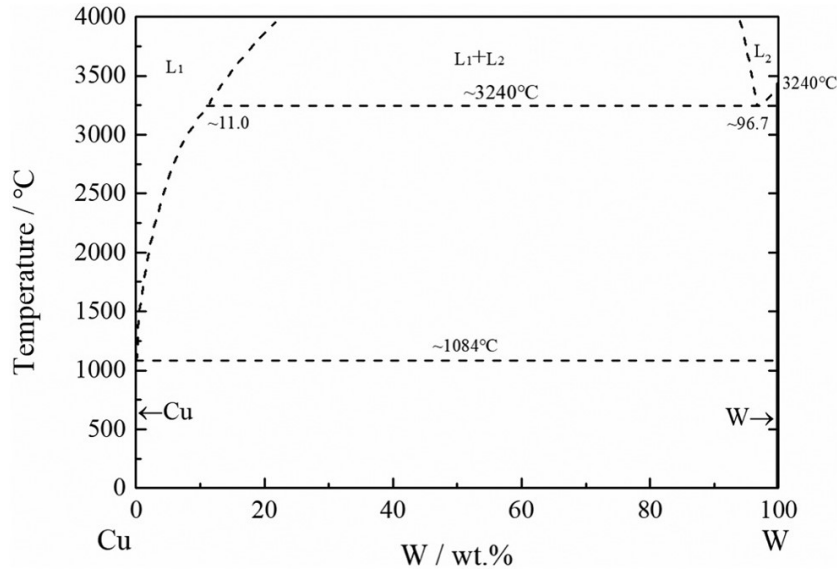


Figure 1: Cu-W binary phase diagram [23]

Tungsten heavy alloys (WHA) contain 90-98 wt% of tungsten and are made from a mix of tungsten powder with other refractory powders like copper, cobalt, nickel and iron. Produced by liquid phase sintering at 1500 °C the composites have density values in the range 17-19 g/cm³, combined with ductility. W-Ni-Cu were the first WHA used, but have since then been replaced by W-Ni-Fe due to the later having superior corrosion resistance and mechanical properties. W-Ni-Fe can be added small amounts of Co to slightly increase both strength and ductility. [14]

2.1.2 Forces during infiltration

Capillary force, P_s , is the main driving force for the penetration of liquid copper into the porous tungsten skeleton. Capillary force can be measured through Eq. 1, where γ_L is the surface tension of molten copper, which at 1150 °C is approximately 1.338 N/m [22]. θ is the wetting angle between molten copper and solid tungsten, which at the same temperature is about 26°. Lastly d is the average diameter of pores in the tungsten. The wetting angle and the surface tension of molten copper during infiltration is shown in Fig. 2.

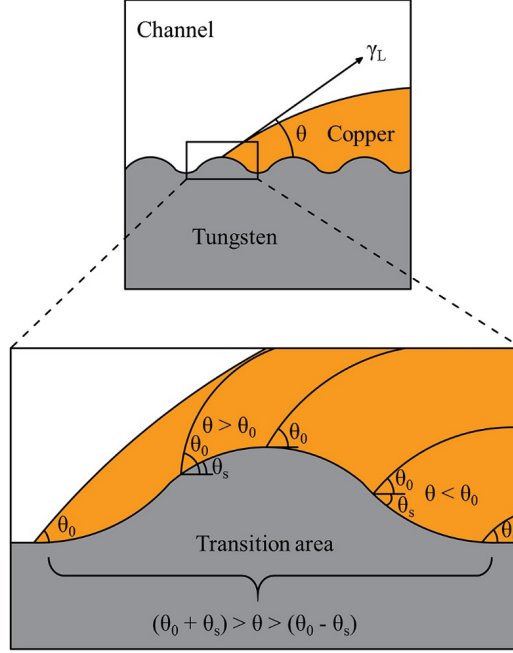


Figure 2: Wetting angle during infiltration. Trend showing the contact angle when liquid copper flows through the tungsten surface with periodic topography. [22]

$$P_s = \frac{4\gamma_L \cos\theta}{d} \quad (1)$$

P_f is the internal friction force which is mainly from adhesion work between molten copper and solid tungsten. Internal friction force can be measured through Eq. 2, where δ is defined as the distance between adjacent linear peaks, which is a measurement of the surface roughness of the tungsten. ϵ is an energy conversion ratio. $\Delta\gamma$ is the surface tension difference between the two phases, which can be assumed to be equal to γ_L [22].

$$P_f = 2\epsilon\Delta\gamma/\delta \quad (2)$$

These two forces are in the magnitude of 10^6 N/m² [22]. Internal friction force works against infiltration, while capillary force in general work for infiltration, but can, when wetting angle exceeds 90° , create resistance towards infiltration (in the case where liquid flows to the ridge). In general these forces work

against one another with the capillary force needing to be greater than the internal friction forces for infiltration to succeed.

The infiltration improves with higher temperatures due to sufficient wetting of tungsten particles by liquid copper and the surface smoothing of the tungsten. Giving the combination of increased capillary force and reduced friction force. [20]

2.1.3 Applications

Tungsten-copper composites can with the combination of properties be used for a wide range of applications including electrodes, arc runners, γ -ray shields, high temperature erosion resistant materials, etc. They are widely used for applications combining high conductivity with high erosion resistance. These include contact materials like ultrahigh-voltage electrical contacts, heat-sink materials and arc resistance electrodes. [6, 14, 22]

2.2 Production of tungsten-copper

2.2.1 Mixing of powder

The production of tungsten-copper composites consist of multiple steps. The first step is mixing of refractory metal powders to achieve desired composition of the tungsten skeleton, for example by wet rod milling. Wax can be added to work as a lubricant, to reduce friction during the pressing. A binder can also be added to increase the strength of the powder mixture. Additives could also be added to the powder(s) at this stage. [1, 14]

2.2.2 Press-sintering

For the second step the powder mixture is pressed forming a green compound. A green compound is defined as compacted powder prior to sintering. The green compound's properties largely determines the properties of the sintered product.[22] An intermediate step for dewaxing and degassing of the green compound can be performed to remove moisture and gases trapped in the pores, by heating up to 450 °C and holding for 30 min.

For the third step the green compound is heated up under vacuum atmosphere to overgo the activation energy for diffusion, initiating solid phase

sintering. During sintering particles bond together into a solid body by diffusion mechanism driven by surface energy reduction.

The sintering is not fully completed, since full density is difficult to achieve for tungsten-copper by sintering. Therefore a skeleton of the desired shape is created with pores which can be filled with copper by mainly two methods; liquid phase sintering and infiltration. [1, 14]

2.2.3 Liquid phase sintering

For liquid phase sintering a blend of refractory metal powders are needed. Typically metal powders combined with tungsten powder are copper, iron, cobalt and nickel. After press-sintering the sintering temperature is set above the solidus of the low-melting component, which give the presence of liquid. Fig. 3 shows a typical temperature-time regime for liquid phase sintering, were the different processes take place.

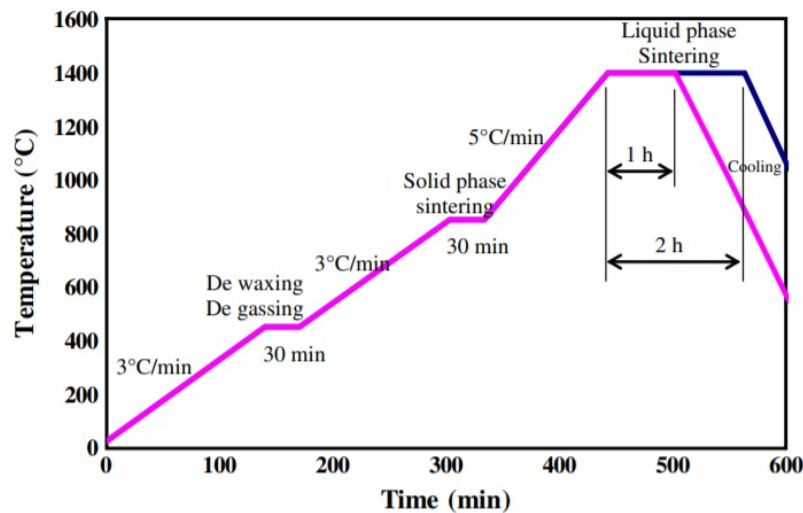


Figure 3: Liquid phase sintering [1]

Abu-Oqail et al. [1] show that relative green density and relative sintered density is increased by increasing copper content. They also show that in-

creasing the sintering time from 1 to 2h, gives samples with both increased hardness and relative sintered density.

2.2.4 Infiltration process

A sample of pure copper metal is placed in contact with the skeleton, and both are heated up above the melting point of the added metal. The added metal liquifies and infiltrates the pores of the skeleton. The result is a highly dense composite of tungsten-copper, which yields 97 % or more of theoretical density. [1, 14, 22]

Instead of using a sample of pure copper for the infiltration step, a sample of pure silver can be used for infiltration of a sintered tungsten skeleton. Silver has a lower melting point than copper, and infiltration temperatures could therefore potentially go even lower. [14]

Zhang et al. [22] tested in their research the use of a layer of covering wax compared to vacuum in the crucible during infiltration. The wax was a mixture of NaCl and KCl powders, which when heated up would create a oxidation stable layer on the surface of the liquid copper. The vacuum had the same effect of protection against oxidation, by evacuation of air. Their results showed that the samples produced in vacuum gave the best properties. They proposed the reason was due to the lower oxygen levels in the crucible compared to the samples covered by wax.

2.2.5 Water-cooling

Lastly the compound is quenched or cooled in water to retain the microstructure. For infiltration an additional step of removing the surplus solid metal is applied. The infiltration process produces the highest density composites for this class of composite materials. An overview of the mentioned processes can be seen in the flowchart in Fig. 4. [1, 22]

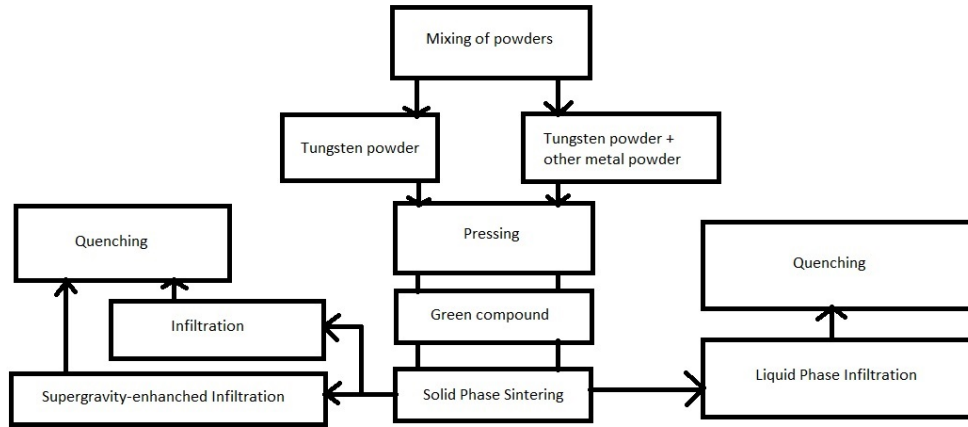


Figure 4: Overview of processes for W-Cu composite production. [14]

2.3 Effects of alloying elements

Alloying elements and additives can be implemented in the powders or added separately during the mixing step. Alloying elements can improve the properties of the material.

2.3.1 Nickel, Cobalt and Iron

The transition elements Ni, Co and Fe can be added to the tungsten powder before pressing. They can segregate in between tungsten atoms, increasing diffusivity of tungsten by creating a transport path. As a result the sintering temperature required is lowered, due to the lower activation energy needed for atomic diffusion.

Another asset of adding these elements is during the infiltration step. Ni, Co and Fe dissolves in the liquid copper, increasing the solubility of tungsten in the liquid copper. The mechanisms for densification rapidly increase with solubility. Therefore inclusion of these elements results in a denser composite.

The setback of using these inclusions is the interaction with the liquid copper, which should be pure to achieve the greatest benefits of the element's properties. Ni, Co and Fe inclusions are especially detrimental for the ther-

mal and electrical properties of the W-Cu composite. Although for the given application, these properties are not of utmost importance. [1, 10, 14, 22]

Cury et al. [5] have looked into possible intermetallic phases (IMP) formed with tungsten, claiming the only stable IMP to be Ni₄W, as other relating literature possible missed the forming of carbides with W and Ni.

2.4 Rule-of-mixtures

The volume fraction of each of the two phases in a composite material determines most of the macroscopic mechanical properties. The rule-of-mixtures depicts a upper and lower limit to give a prediction of mechanical properties based on the mechanical properties of the constituents. For the estimation of elastic modulus equation (3) og (4) can be used, giving the upper and lower limit respectively [4].

$$E_c(u) = E_m V_m + E_p V_p \quad (3)$$

$$E_c(l) = \frac{E_m E_p}{V_m E_p + V_p E_m} \quad (4)$$

E and V denotes in these equations the elastic modulus and the volume fraction, respectively. The subscripts c , m and p corresponds to composite, matrix and particulate phases, respectively. Other macroscopic mechanical properties can be estimated similarly.

2.5 Recycling

Theory regarding the tungsten extractive metallurgy and recycling were also included in the scope of the work by the request of Sandvik Teeness. On the path towards industrialisation, it is important to have a understanding of how to handle components at the end-of-life and how the elements can be recovered and/or recycled as part of a circular economy. Tungsten is a critical element [8] and therefore needs to be treated accordingly.

Tungsten-bearing scrap can be used as an alternative to minerals for production of new tungsten metal powder. In general tungsten components of high tungsten content are therefore recyclable. The tungsten scrap is firstly crushed by high energy mills. From here it can either be directly re-used for

lower quality applications, used as additions to steel for alloying or can be oxidized followed by reduction to create new powder at a much lower cost than production from minerals. The last case is known as chemical recycling.

After the oxidation the tungsten is in the form of tungsten trioxide (WO_3) and tungstates of nickel, cobalt and iron. These are then reduced as feed material for ammonium paratungstate (APT), which is further reduced through multiple steps to produce pure tungsten powder.

For composite scrap mixtures, which is the case for W-Cu composites, the scrap is difficult to oxidize, making chemical recycling not applicable. For the case of using the scrap as alloying additions in steel, this is not recommended, due to the detrimental properties of copper in steel. A possible solution could be to use salt melt digestion, using mixtures of sodium nitrate, sodium nitrite and sodium carbonate. The problem with this solution is the environmental issues of formation of nitrous gases. A proposed solution is to use electrochemical recovery of the tungsten. [14]

2.5.1 Raw tungsten resources

Tungsten show an increasingly demand for use in manufacturing and process industries worldwide, focused around emerging economics. The primary resources include scheelite (CaWO_4 , 80.5 % WO_3) and wolframite ($(\text{Fe,Mn})\text{WO}_4$, 76.3-76.6 % WO_3).

The following figures show different methods for production of tungsten powder.

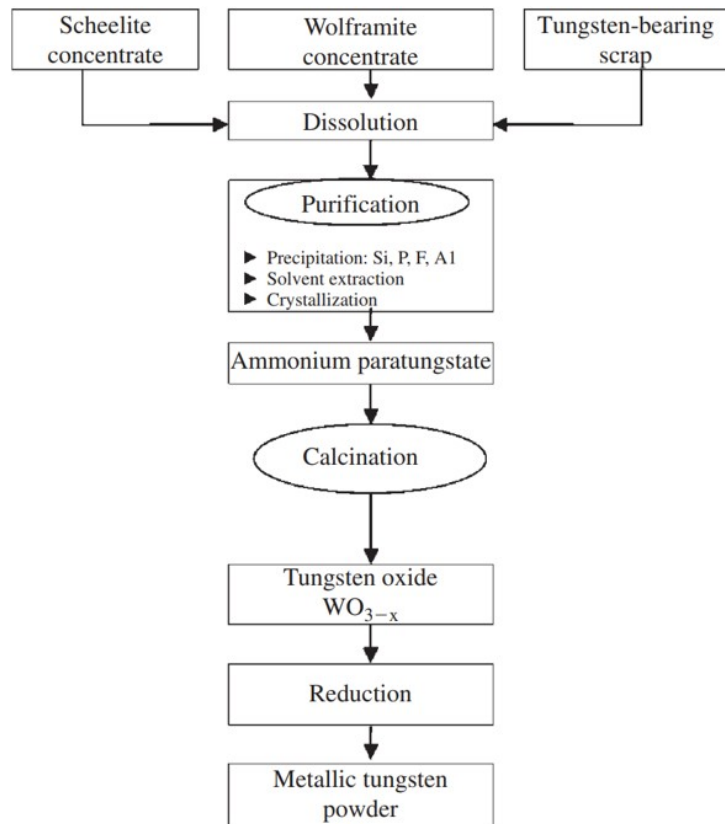


Figure 5: Tungsten metal powder production route. [14]

Fig. 6 show the production route for APT using the hydrochloric acid process. This method has been used since the early 1960s.

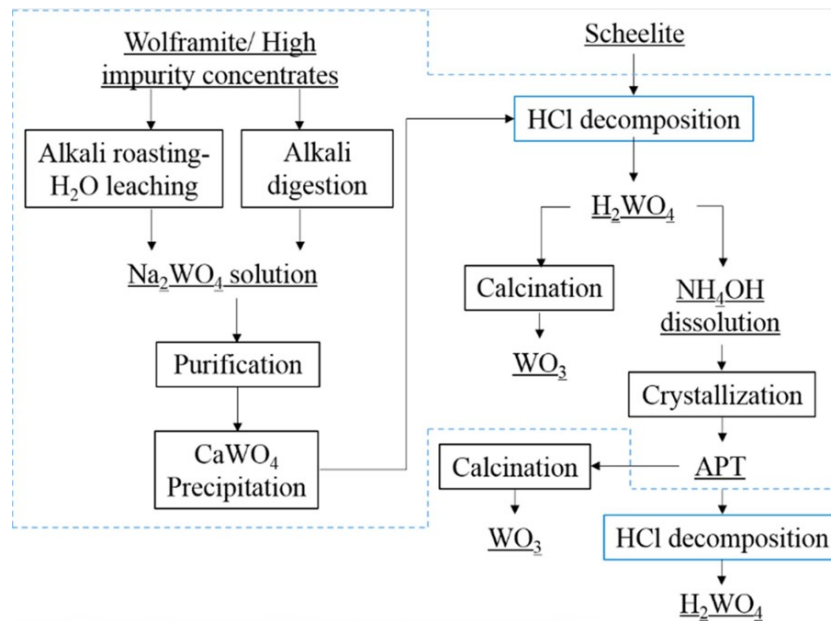


Figure 6: Hydrochloric acid process for production of APT.[17]

Fig. 7 show the production route for APT using the solvent extraction production. This method is primarily used in Europe and the USA.

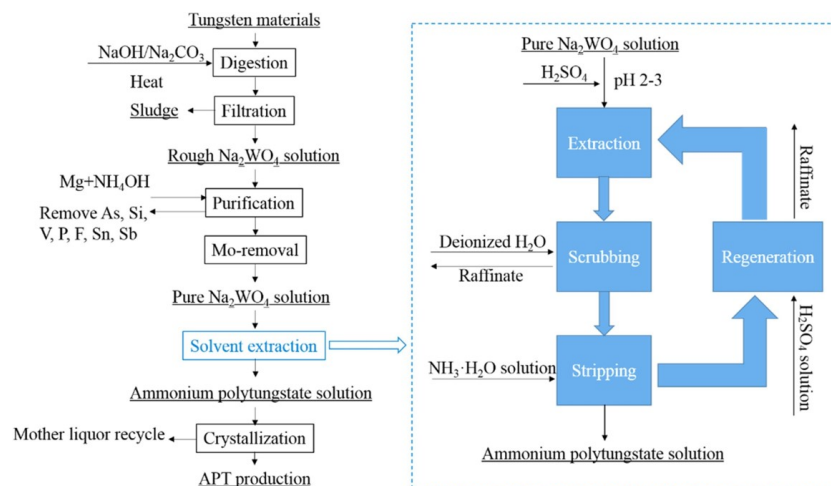


Figure 7: Solvent extraction process for production of APT.[17]

Fig. 8 show the production route for APT using the ion exchange production. This method is primarily used in China.

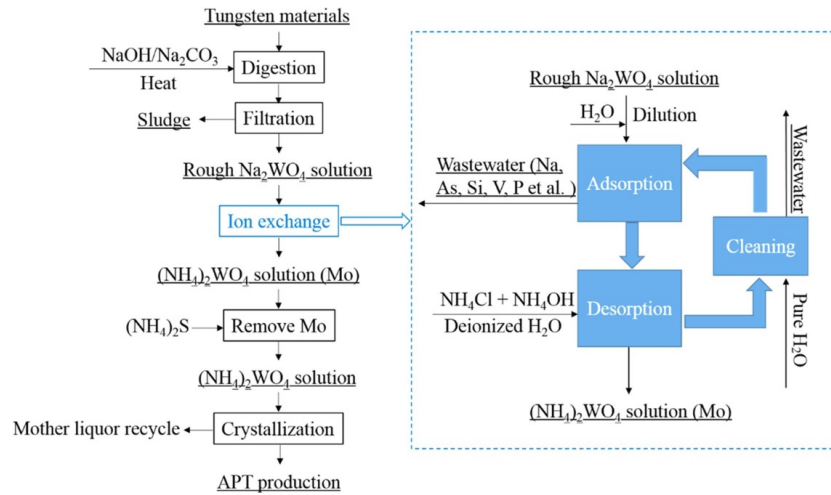


Figure 8: Ion exchange process for production of APT.[17]

As seen in Fig. 9, approximately 66% of tungsten is produced by primary sources. In Europe and the USA is there and even higher portion of secondary sources used.

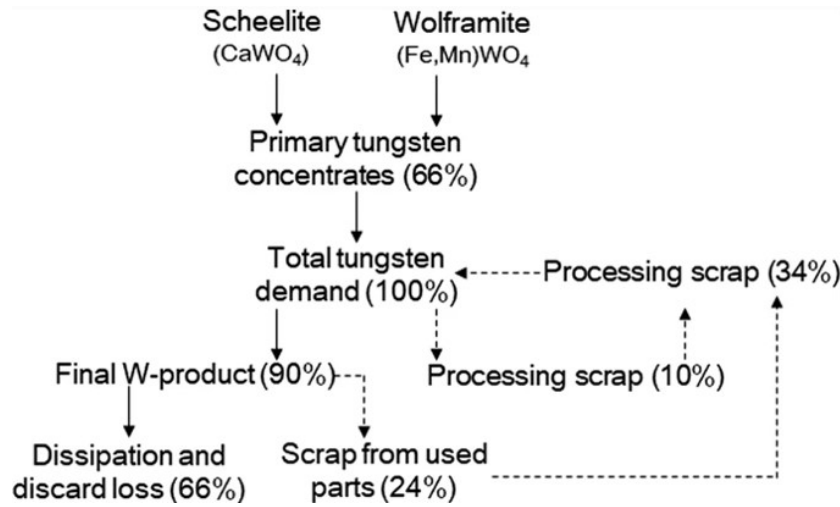


Figure 9: Tungsten flow cycle.[19]

Tungsten concentrates need to undergo pretreatment to ensure a stable production, by removing organics and impurities. The pretreatment could be roasting at $\approx 650^\circ\text{C}$, leaching by submerging the concentrates in an alkali solution or dilute inorganic acid, or by a combination of the two processes. The most recent methods include roasting transformation- $(\text{NH}_4)_2\text{CO}_3$ leaching and H_2SO_4 conversion-ammoniacal $(\text{NH}_4)_2\text{CO}_3$ leaching dated from 2014 and 2016 respectively.

2.5.2 Overview of recycling methods

Recycling of tungsten scraps can be divided into three groups of: Direct recycling, indirect recycling and semi-direct recycling.

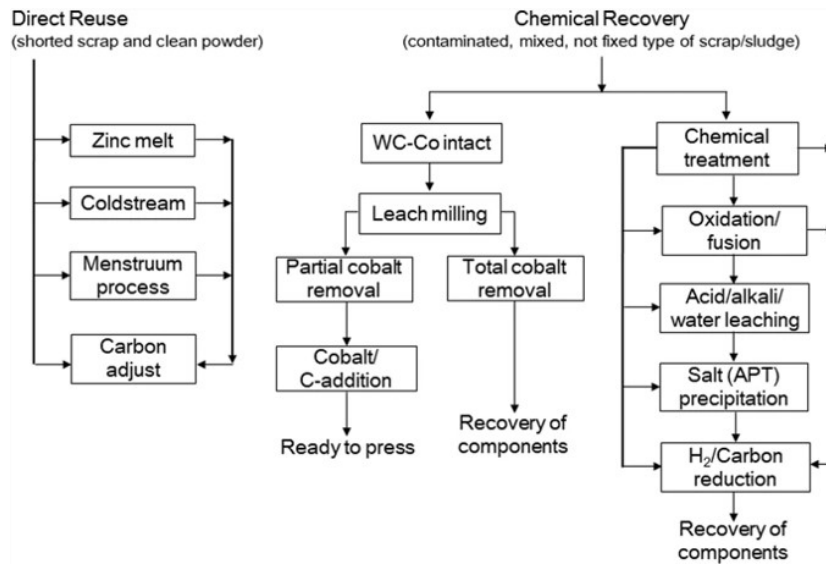


Figure 10: Overview of recycling scheme.[19]

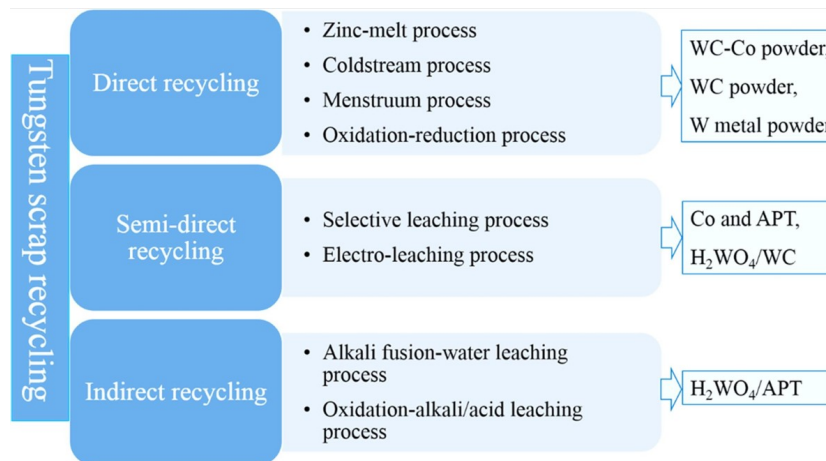


Figure 11: Overview of recycling from tungsten scraps.[17]

The direct methods gives high recovery, good quality powder and good grain size control. However on the downside, direct methods have incomplete separation of metal carbides from the binder material. Therefore they require specialized, costly equipment and they are very energy intensive. [16]

The use of zinc-melt process have been claimed to give successful recycling of W-Cu and W-Ag scraps into metal powder by The Kohsei Co., Ltd. (Japan) [11, 19]

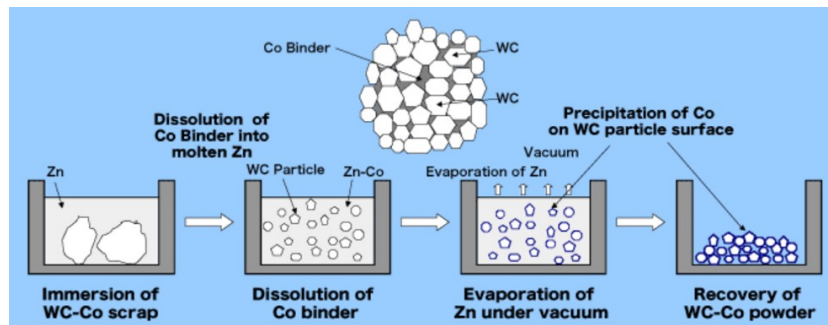


Figure 12: Overview of the zinc-melt process. The method is primarily used on WC-Co scrap, resulting in the recovery of alloyed WC-Co powder. The Kohsei Co., Ltd. have claimed the method to be applicable also on W-Cu and W-Ag composites. [11]

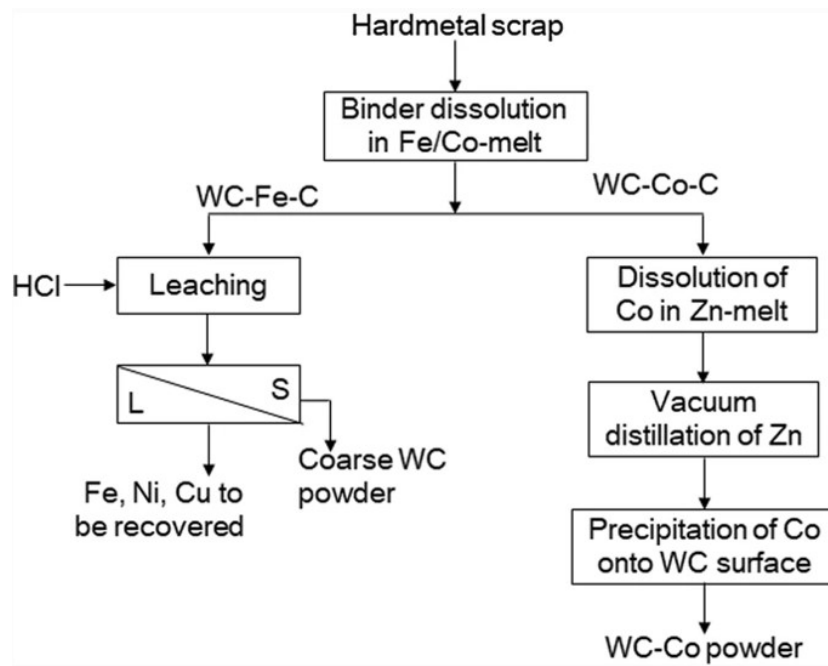


Figure 13: Menstruum process.[19]

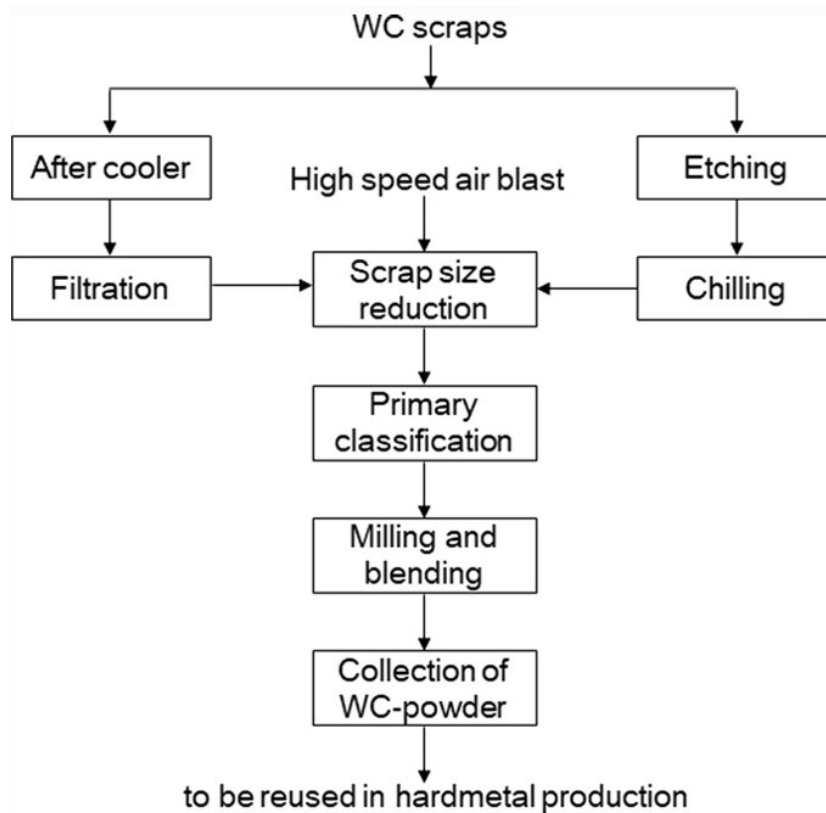


Figure 14: Cold stream process.[19]

Indirect methods produce APT, with the chemical formula of $(\text{NH}_4)_{10}(\text{H}_2\text{W}_{12}\text{O}_{42}) \cdot 4\text{H}_2\text{O}$. APT is the most important precursor for all tungsten intermediate products. Tungsten trioxide (WO_3), tungsten blue oxide (BTO), tungsten acid, $\text{H}_2\text{WO}_4 \cdot n\text{H}_2\text{O}$, and ammonium metatungstate, $(\text{NH}_4)_6(\text{H}_2\text{W}_{12}\text{O}_{40}) \cdot 3\text{H}_2\text{O}$, are the most common products synthesised. Figure ITIA shows the different production routes for producing each of the final products.

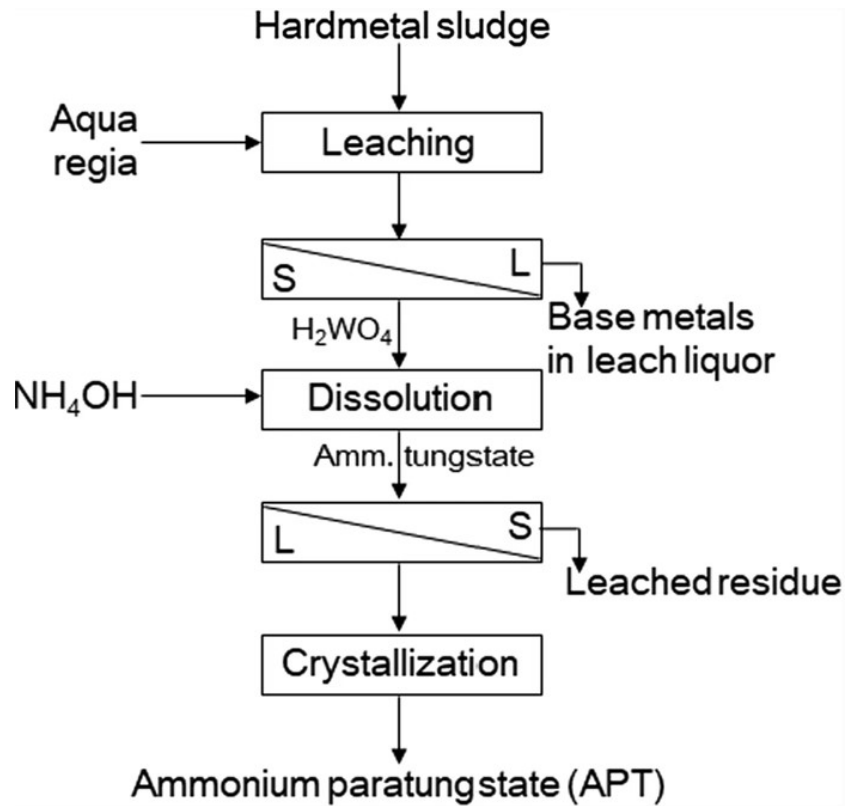


Figure 15: Overview of leaching with aqua regia used for dissolving WC-Co composites. Aqua regia also dissolves Cu, which makes the method also applicable on W-Cu composites. [19]

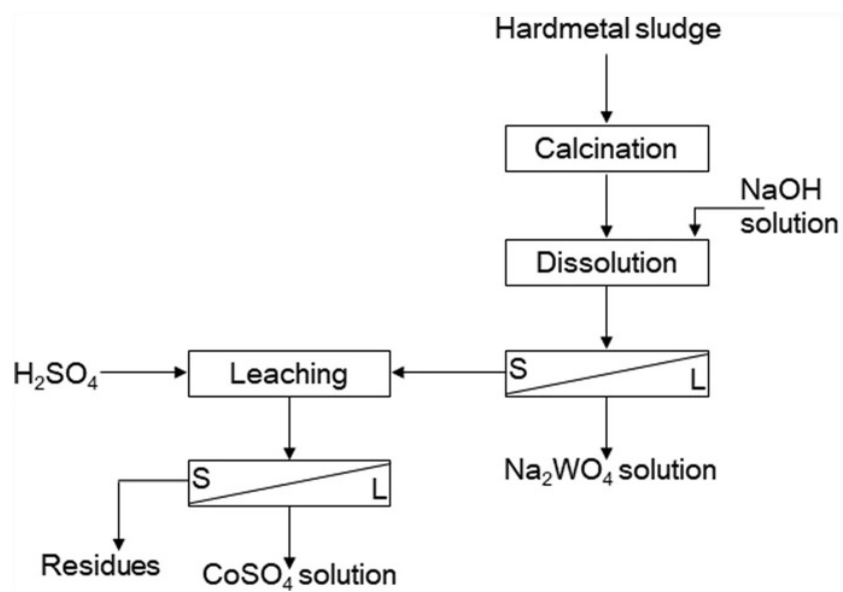


Figure 16: Calcination followed by alkali leaching process.[19]

3 Experimental

The experimental work were focused on the mechanical properties of infiltrated samples manufactured at Sandvik. Tensile test specimens were milled out from three different samples, namely Sn 2, Sn 13 and Ni 1. The experimental work will be presented in this section, explaining the procedure and methods used.

The two former samples, Sn 2 and Sn 13, are made by infiltrating tungsten with (tin) bronze powder and with a (tin) bronze piece respectively. The samples are distinguished by covering different ranges of density, in accordance to the two ranges specified by Sandvik's product range (11-13 g/cm³ and 13-15 g/cm³ for Sn 2 and Sn 13 respectively). The tungsten powder used for the two samples also differ. The Ni 1 specimen was made by infiltration of copper powder through compacted nickel powder into compacted tungsten, as seen in Fig. 17. The crucible used was made from 314 stainless steel. The configuration is obtained from Sandvik.

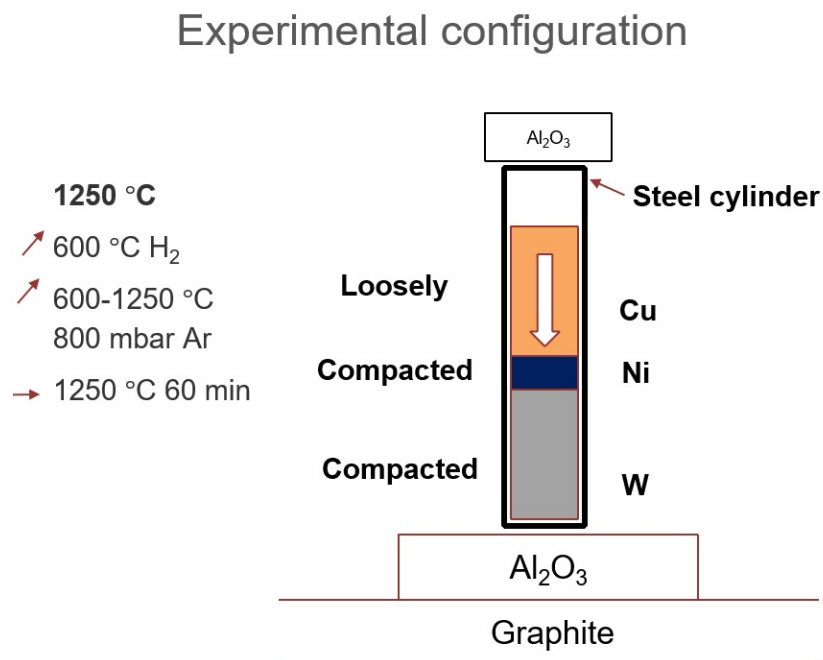


Figure 17: Experimental configuration of infiltration of the Ni 1 sample

These three samples were compared by tensile testing, Computerized Tomography (CT) scan before and after tensile testing, microstructure observed in Optical Microscope (OM) and Scanning Electron Microscope (SEM), composition analysed with Energy-Dispersive X-ray Spectroscopy (EDS), hardness measured and fracture surface observed in macroscope. Overview of experimental data for the three different samples is listed in [Table 1](#).

Table 1: Experimental data for each of the three samples

Powder/piece	<i>Sn 2</i>	<i>Sn 13</i>	<i>Ni 1</i>
W powder	314.8g Technon -100 Mesh	186.1g Residual	452.93g Technon -100 Mesh
Bronze powder	96.6g ExOne CuSn10		
Bronze piece		138.0g CuSn12	
Cu&Ni powder			257.0g

Bronze samples were produced at 1170 °C for 6 hours in vacuum atmosphere. The difference in Sn content between the bronze powder and the bronze piece, marks a difference in microstructure. For $\leq 11\%$ Sn have the α -phase. Alloys with 11-18% Sn have the α -phase but also hard, brittle δ -particles are present.[18]

The Technon W powder have particle size noted by -100 Mesh, which means the powder have been passed through a 100 mesh screen, which gives the maximum particle size of 149 μm [13]. The Residual W powder consists of a wider range of particle sizes.

3.1 Sample Preparation

For OM analyses two tensile test specimens from each sample series were chosen. The microstructure were assessed from tensile test specimens after testing, both from the bottom, unaffected by the test, and in the fracture area. For the former analyses, tensile test specimens were casted in epoxy, by mixing of 41.08 g EpoFix resin with 4.92 g EpoFix hardener and stirring the mix for 120 seconds with variable motions. The mix were then distributed among two small castings with a diameter of 25 mm for Sn 2 and Sn 13 samples and one large casting with a diameter of 40 mm for the Ni 1 sample. A larger casting were used for the Ni sample to be able to submerge the whole piece. The epoxy hardened overnight under fume hood.

For studying the microstructure in the fracture area, the tensile tip were cut from the rest of the fractured tensile test using Struers Accutom-5 cutting machine with Struers High Quality Cut-Off Wheel 10S15 blade. For these

samples small castings of 25 mm were used for all three specimens, which were filled with aluminium foil. The tensile tip were laid at level with the base of the cast as seen in Fig. 18 below. A grinding pre-step were used to remove epoxy until above ≈ 1 mm of the tensile tip, the subsequent grinding steps would then result in the revealing of the microstructure across the fracture area.

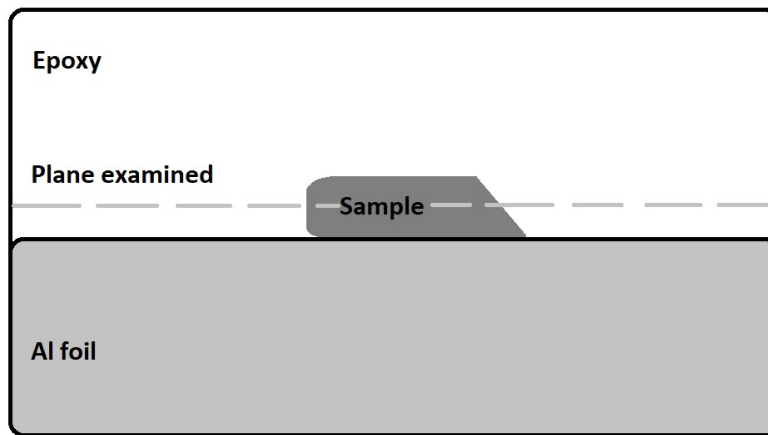


Figure 18: Setup for casting in epoxy for fracture area analyses. The marked plane to be examined is revealed after both the grinding and polishing steps have been executed.

For the grinding of samples, SAPHIR 330 semi-automatic machine were used with 150 rpm rotation and water as lubrication. SicFoil with grit 800 were applied on MD Gekko disc. For the fracture analysis samples, the pre-step used SicFoil with grit 500, maintaining other parameters.

Struers Tegramin-30 were used for further grinding and polishing of samples. For all steps a rotation of 150 rpm were used. For grinding MD molto 220 were used first with a force of 30 N for 4:00 minutes. Secondly MD Largo with DiaPro Allegro Largo 9 were used with the force set to 15 N. For this step a 3:00 min pass were sufficient.

For polishing MD Mol with DiaPro Mol R3 were used first, polishing down to $3 \mu\text{m}$. For this step one pass of 6:00 min were used with the force set to 10 N. Secondly MD Nap with DiaPro Nap R1 were used, polishing down to $1 \mu\text{m}$. For this step two passes of 10:00 min were needed with the force set

to 10 N. The samples were rinsed between each step and after each polishing step the samples were also cleaned with ethanol and air-dried using hair dryer.

3.2 Material properties

3.2.1 Density

The density is an important property of infiltrated composites, both as a measurement of porosity when compared with theoretical density (important for analysing efficiency of the infiltration process), and due to the high density of tungsten, the density of the composite gives the mechanical properties based on the volume fraction of tungsten (see section 2.4)

The density measurements were conducted by applying Archimedes' law by submerging the tensile tests in water (see Fig. 19). Specimens were first weighted on a Sartorius CP3202S metallurgical weight with an accuracy of ± 0.01 g. A measuring cylinder of 10 mL was filled with water and volume with accuracy of ± 0.01 mL were read on the measuring cylinder, firstly without and then with tensile test specimen. The density were calculated according to equation (5), where ρ_c is the bulk density, m is the mass and ΔV is the calculated volume of the specimen, by subtracting the initial volume from the volume with the specimen submerged.

$$\rho_c = m/\Delta V \quad (5)$$



Figure 19: Setup for the density measurements using Archimedes' principle.

3.2.2 Tensile Testing

Tensile stress-strain testing is used to determine the tensile properties of a material. A specimen is deformed to fracture by gradually increasing an uniaxially load along the long axis of the specimen. The force and change in length is measured, resulting in a stress-strain curve which has shape and magnitude depending on the material tested. For engineering stress-strain curves, the stress and strain depend on the initial cross-sectional area and the initial length measured by extensometer respectively.

The stress-strain curves are used for determining the mechanical properties yield strength (YS), ultimate tensile strength (UTS), fracture strength, elastic modulus and corresponding strain values including the total elongation. The curves are also used for determining whether the material is brittle or ductile.

Tensile test specimens were milled out at Sandvik after the specification given below in [Fig. 20](#). The cylindrical shape was chosen due to giving better results in CT scan.

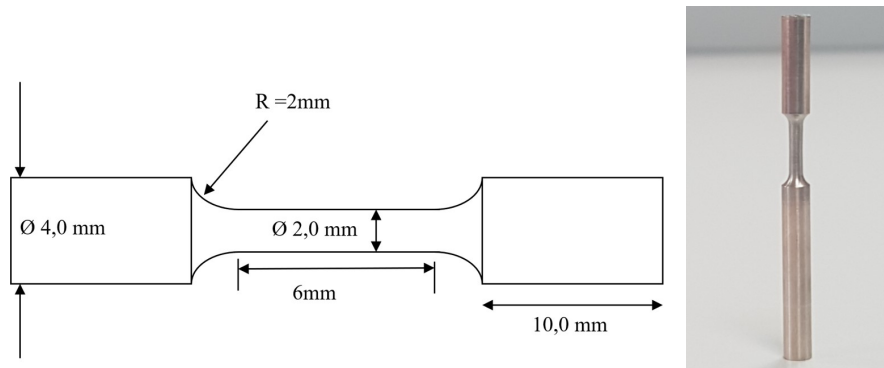


Figure 20: Tensile test specimen specification for cylindrical specimen.

Four parallel tensile tests for each of Sn 2 and Sn 13 samples were carried out, while for the Ni 1 sample, a total number of seven parallel tests were carried out. The higher number of tests for Ni 1 were due to several less optimal tests, which resulted in fracture outside the measuring area of the video extensometer. This resulted in negative change in strain values. For these curves data points up until this point, is the only data points applied in the results.

Because of limited access to labs during the semester due to the covid-19 pandemic, the tensile testing were carried out by Chief Engineer Pål Christian Skaret at the Department of Materials Science and Engineering. The tensile tests were carried out using a Zwick/Roell 2,5 kN apparatus with a Videoextens laser-video extensometer. A strain rate of 0.2 mm per minute was applied.

The diameter of the cross-sectional area were measured by Pål Christian Skaret prior to testing and by the author after testing. The specimens were quite accurately milled to a diameter of 1.95 ± 0.01 mm. The values were used to determine the reduction of area, q , during each of the tensile tests.

3.2.3 Hardness

Hardness was measured with Zwick Roell ZHV30 Vickers hardness tester. Measurements were taken using a Free Run option in the software to be able to measure the tungsten and copper phases distinctly. The dwell time was set to 10 seconds. The indents were aimed to have diameters with size in the range 100-150 μm , to give the most accurate results with the equipment.

Through trial and error the diameter in the given range were found to be obtained from using a force of 1 kg for the copper phase. For the tungsten phase the closest results to the desired indent size were found to also be 1 kg, due to the apparatus having limited options of available loads. For future work a force of 2 kg is recommended. Hardness was measured on each of the samples examined in OM. One specimen for each of the three samples Sn 2, Sn 13 and Ni 1 were tested. The hardness was tested both in the unaffected zone and in the fracture area (but performed on different tensile tests). Five measurements of each of the two phases in each specimen were taken, giving a total of ten measurements for each of the specimens tested.

3.3 Microscopy

3.3.1 Macroscope

The Macroscope Leitz Wild were utilised to receive an overview of the fracture area of the tensile test specimens after fracture. The three light sources Intralux 5000, Intralux 6000 and Intralux 150H were used. Images were taken with 20x magnification on the Makrozoom lens used. The ocular yielding 10x magnification gives a total of 200x magnification. Images were taken of both parts of tensile test specimen after fracture for every specimen tested in tension. A copy paper were used to limit light from other light sources in the room. The setup is seen in [Fig. 21](#).



Figure 21: Macroscopic setup

3.3.2 Computerized Tomography (CT)

The CT scans were conducted by Staff Engineer Ole Tore Buset. One specimen of each sample were scanned both before and after tensile testing. For the latter the pieces were pinned together by tape, and the fracture area were examined. For the scans performed prior to tensile testing, the specimens were examined in 2D layers aligned with the cross-sectional area throughout the whole specimen. The cylindrical shape of the tensile test specimens were chosen to have a smaller cross-sectional area, to give better scanning results.

3.3.3 Optical Microscope (OM)

OM was used to examine the microstructure of the samples, both in the unaffected zone (microstructure after infiltration) and in the fracture area (after tensile testing). One specimen for each sample were examined. The optical microscope LEICA MEF4M were used with ProgRes CapturePro software. Images were taken with magnification set to 2.5x, 5x, 10x, 20x, 50x and 100x. With the ocular yielding 10x magnification, the total magnification were 25x, 50x, 100x, 200x, 500x and 1000x respectively.

3.3.4 Scanning Electron Microscope (SEM)

SEM uses a thin beam of electrons to analyse electrically conducting samples. When interacting with the surface atoms of the sample, an array of signals can be detected, with the main being secondary electrons, backscattered electrons and x-rays.

Zeiss Supra 55VP LVFESEM was used for the SEM images, as well as the EDS scans. The apparatus is a low vacuum field emission SEM yielding high resolution. SEM images were taken using secondary electron detector. The secondary electron detector was used since the signal comes from a small emission volume, it is well suited for imaging the surface and describe the topography. EHT were set to 10 kV, aperture size to 30 μm , high current off, working distance set to close to 20 mm. Images of each samples were taken with 50x, 200x, 300x, 400x, 500x and 1000x magnification, with more images on the higher magnification to highlight different areas in the fracture surface.

3.3.5 Energi-Dispersive X-ray Spectroscopy (EDS)

For the EDS scans a SEM image of the sample were taken with increased electron high tension (EHT), larger aperture size set to 120 μm , high current on and working distance set to 10 mm. The EHT was increased to increase the energy of the primary electrons. Voltage needs to be higher than the critical excitation voltage to be able to excite atoms. When returning to ground state, the atoms emits characteristic x-rays. For L-radiation, tungsten have a excitation potential of about 10 kV [9]. EHT was set to 20 kV to ensure high enough energy of the primary electrons to get sufficient radiation. Both EDS Point scan and EDS Mapping were conducted using the TEAM Enhanced software. Some elements showing trace amounts were removed from the quantitative analysis, as deemed negligible.

4 Results

In this section the experimental results will be presented. The results will be compared and discussed in section 5.

4.1 Density

Fig. 22 shows the values read from the measuring cylinder and the resulting densities calculated. As can be seen when comparing the two last columns, there are some discrepancies between the average measured density, ρ_{avg} , and the density of the infiltrated sample before milling to tensile test specimens, measured at Sandvik, $\rho_{Sandvik}$.

Material	Sample	Weight [g]	V ₀ [mL]	V [mL]	ΔV [mL]	ρ_c [cm ³ /mL]	ρ_{avg} [cm ³ /mL]	$\rho_{Sandvik}$ [cm ³ /mL]
W-bronze	2,1	4,91	6,73	7,07	0,34	14,44	15,55	14,9
	2,2	4,79	6,13	6,43	0,30	15,97		
	2,3	4,89	6,69	7,00	0,31	15,77		
	2,4	4,81	6,51	6,81	0,30	16,03		
	13,1	4,13	6,20	6,55	0,35	11,80	11,56	12,63
	13,2	4,06	7,63	8,00	0,37	10,97		
	13,3	4,05	6,12	6,49	0,37	10,95		
	13,4	4,13	6,77	7,10	0,33	12,52		
W-Cu-Ni	1,1	6,85	6,37	6,82	0,45	15,22	12,67	
	1,2	6,81	7,20	7,78	0,58	11,74		
	1,3	6,83	7,11	7,60	0,49	13,94		
	1,4	6,83	6,09	6,73	0,64	10,67		
	1,5	6,83	6,78	7,34	0,56	12,20		
	1,6	6,82	7,21	7,72	0,51	13,37		
	1,7	6,76	5,75	6,28	0,53	12,75		
	1,8	6,75	7,41	8,00	0,59	11,44		

Figure 22: Density measurements by Archimedes' law

Values for density of pure elements were accessed from *Materials Science and Engineering SI Version* [4]. At 20 °C the density is 19.3, 8.94, 8.90 and 7.27 g/cm³ for W, Cu, Ni and Sn respectively. The theoretical density of the samples were measured according to equations (6)-(8). For the bronze samples, the theoretical density of the bronze component were firstly calculated using the same equations with Cu substituting W and Sn substituting Cu in the formulas. The resulting theoretical density value for the bronze were then used for the density of Cu used in the equations for the calculations for theoretical density of the W-bronze composite. For the Ni 1 sample, the dissimilarity between the density of Cu and Ni were deemed negligible. The calculations followed therefore the equations as they stand.

$$V_{tot} = \frac{100 \cdot C_W}{\rho_W} + \frac{100 \cdot (1 - C_W)}{\rho_{Cu}} \quad (6)$$

$$V_W = \frac{\frac{100 \cdot C_W}{\rho_W}}{V_{tot}} \quad (7)$$

$$\rho_s = \rho_W V_W + \rho_{Cu}(1 - V_W) \quad (8)$$

In equation (6)-(8) the V_{tot} is the volume of 100 g of composite, V_W is the volume fraction of tungsten, C_W is the weight percentage of tungsten and ρ_W , ρ_{Cu} & ρ_s is the density of W and Cu and the theoretical density of the composite respectively. The relative density, ρ_d , was measured using equation (9), where ρ_c is the bulk density measured by Archimedes' law. The results are put together in Table 2.

$$\rho_d = \frac{\rho_c}{\rho_s} \cdot 100\% \quad (9)$$

Table 2: Density calculations

Property	<i>Sn 2</i>	<i>Sn 13</i>	<i>Ni 1</i>
ρ_c [g/cm ³]	15.55 ± 0.75	11.56 ± 0.75	12.67 ± 1.47
ρ_s [g/cm ³]	15.05	12.72	13.61
ρ_d [%]	103.38	90.85	93.05

4.2 Tensile tests

A total of four, four and seven tensile tests were conducted for the Sn 2, Sn 13 and Ni 1 samples respectively. The results for each of the samples were compared separately in Fig. 23, Fig. 24 and Fig. 25 respectively. The material specification given in section 1.2 corresponds to a engineering stress-strain curve with steep increase in stress in the elastic region, followed by high fracture strain giving long total elongation.

The material specification for the elastic modulus has been incorporated in the plots to more easily compare the elastic modulus of the specimens tested with the material specification. The stress-strain curves should be along or to the left of the dotted line to fulfill the criteria, in the elastic zone.

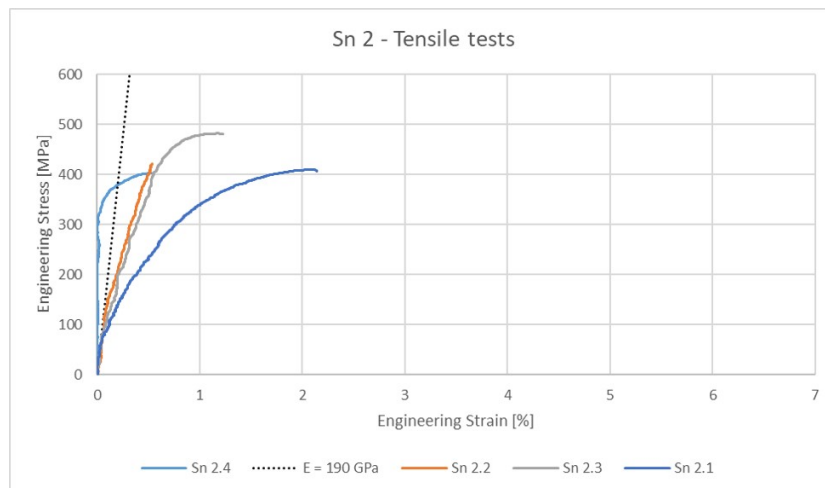


Figure 23: Tensile tests of the Sn 2 sample.

As can be seen in Fig. 23, the specimens show a large variation in elastic modulus, high strength and the Sn 13.1 specimen is distinguished with a much larger fracture strain than the other specimens tested. The elongation for all of the specimens is quite low. The Sn 2.4 specimen shows the highest elastic modulus, but this is due to little response from video extensometer during testing. The strain values are therefore higher than shown in the plot, giving a lower value for elastic modulus than measured.

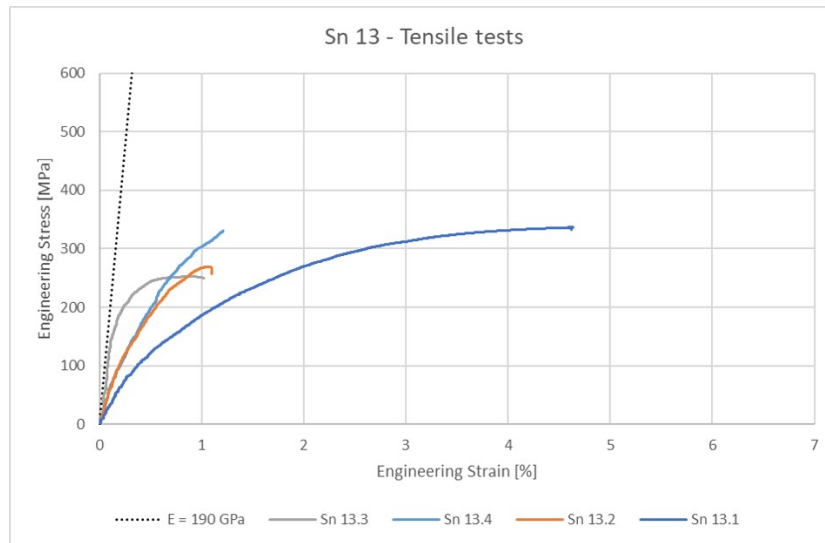


Figure 24: Tensile tests of the Sn 13 sample.

The most notable feature seen in Fig. 24 is the low elongation for three of the specimens, while the last shows longer elongation almost reaching the material specification of 5%. Another noticeable feature is the variation in elastic modulus, ranging from satisfactory to far off from the material specification (marked by the dotted line in the figure). Compared to Sn 2 tensile tests, one can also notice the lower yield and ultimate tensile strengths for the Sn 13 specimens.

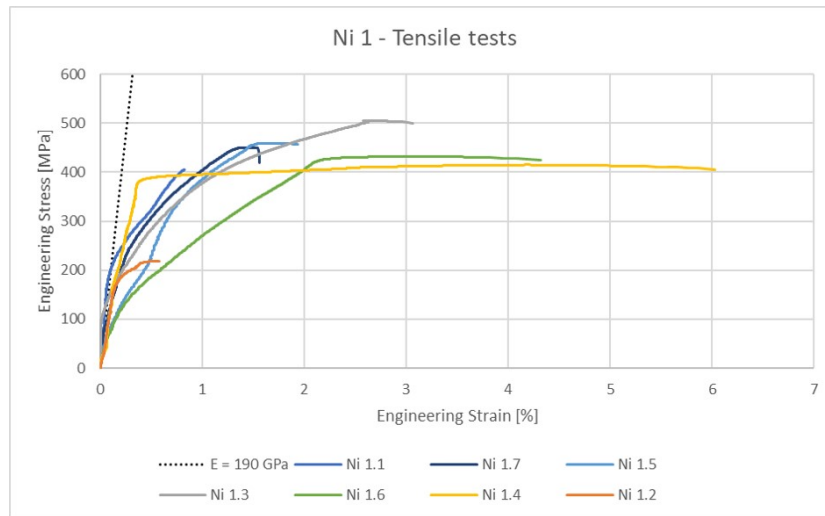


Figure 25: Tensile tests of the Ni 1 sample.

The most notable feature in Fig. 25 is the larger elongation of specimens, compared with both Sn 2 and Sn 13 tests, but with a large variance in the results. Most of the specimens also show large yield and ultimate tensile strengths. The Ni 1.4 tensile curve shows the desirable shape to satisfy the material specifications, having the largest elongation and high strength. The numerical results from the tensile tests are summarized in the table in Fig. 26. The average and the standard deviation of the material properties in Fig. 26 are summarized in Table 3.

Sn-samples	E-modulus [Gpa]	R _{p0.2} [MPa]	A _{tot} [%]
2,1	45,54	299,89	2,15
2,2	72,68	443,25	0,54 **
2,3	64,63	470,06	1,22
2,4	170,91	405,50	0,53 **, ***
13,1	29,78	147,60	4,62
13,2	67,18	184,06	1,09
13,3	47,78	251,11	1,02
13,4	41,01	282,93	1,21 **
Material specification	190,00	200,00	5,00
Ni-samples	E-modulus [Gpa]	R _{p0.2} [MPa]	A _{tot} [%]
1,1	227,60	281,74	0,82
1,2	120,00	210,00	0,58 *
1,3	35,98	370,96	3,07 *
1,4	95,00	392,50	6,03 *
1,5	38,74	410,33	1,94
1,6	92,77	162,24	4,32
1,7	76,72	341,00	1,56
Material specification	190,00	200,00	5,00
*Fracture in the radius			
**Data from before curve turns back only, due to fracture outside area of measurement			
***Little response from videoextensometer			

Figure 26: The resulting numerical data from the tensile tests for all of the samples.

Table 3: Tensile properties of the samples with standard deviation.

Property	Sn 2	Sn 13	Ni 1
E-modulus [GPa]	88.44 ± 56.14	46.44 ± 15.70	98.12 ± 64.72
R _{p0.2} [MPa]	404.67 ± 74.71	216.42 ± 61.67	309.83 ± 95.03
A _{tot} [%]	1.11 ± 0.76	1.99 ± 1.76	2.61 ± 1.99

4.3 Reduction of area (q)

The reduction of area, q , is a measurement of ductility of the material and is independent of both initial area and initial length of the specimen. q is calculated by using equation (10). The results are shown in Fig. 27.

$$q[\%] = \frac{A_0 - A_f}{A_0} \cdot 100\% \quad (10)$$

Material	Specimen	q [%]
W-bronze	2,1	0,00
	2,2	-3,32
	2,3	0,00
	2,4	0,00
	13,1	0,51
	13,2	-2,72
	13,3	0,00
	13,4	0,00
W-Cu-Ni	1,1	1,02
	1,2	-0,24
	1,3	2,75
	1,4	0,00
	1,5	0,51
	1,6	0,51
	1,7	2,55

Figure 27: Reduction of area during tensile testing. Notice how the Ni sample shows higher values for q than both of the two bronze samples.

For engineering tensile curves the stress decreases beyond the ultimate tensile strength (UTS). This is due to the phenomenon known as necking, where the cross sectional area is reduced. The larger the reduction of area, the more plastic deformation the material undergoes before initiating fracture. The larger value for q, the more ductile the material is. The distinction between brittle and ductile material lies around 5% total elongation [4], which corresponds with the material specification given by Sandvik.

4.4 Hardness

The hardness was examined for two different areas in the specimens analysed, with one specimen for each sample tested. The unaffected zone corresponds to the microstructure not being altered by the tensile testing, and were access from polishing the bottom end of the specimen. The fracture area were revealed by polishing according to Fig. 18.

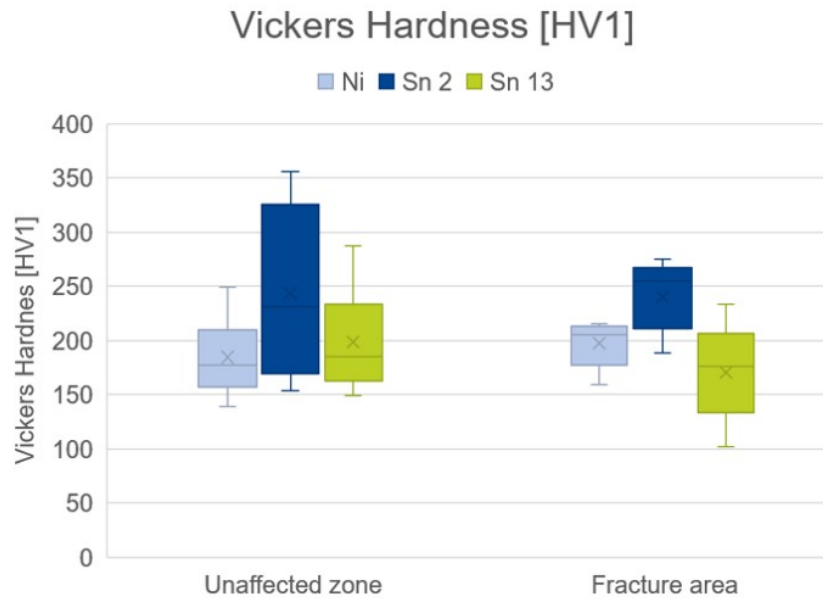


Figure 28: Hardness measurements of all three samples.

4.5 Macroscopic

A total of four, four and seven tensile tests were conducted for the Sn 2, Sn 13 and Ni 1 samples respectively. In the macroscopic the fracture area were examined. In Fig. 29-31 image a)-g) corresponds to tensile tests Ni 1.1-Ni 1.7 for the Ni 1 sample respectively. Similar notation are used for the Sn 2 and the Sn 13 samples.

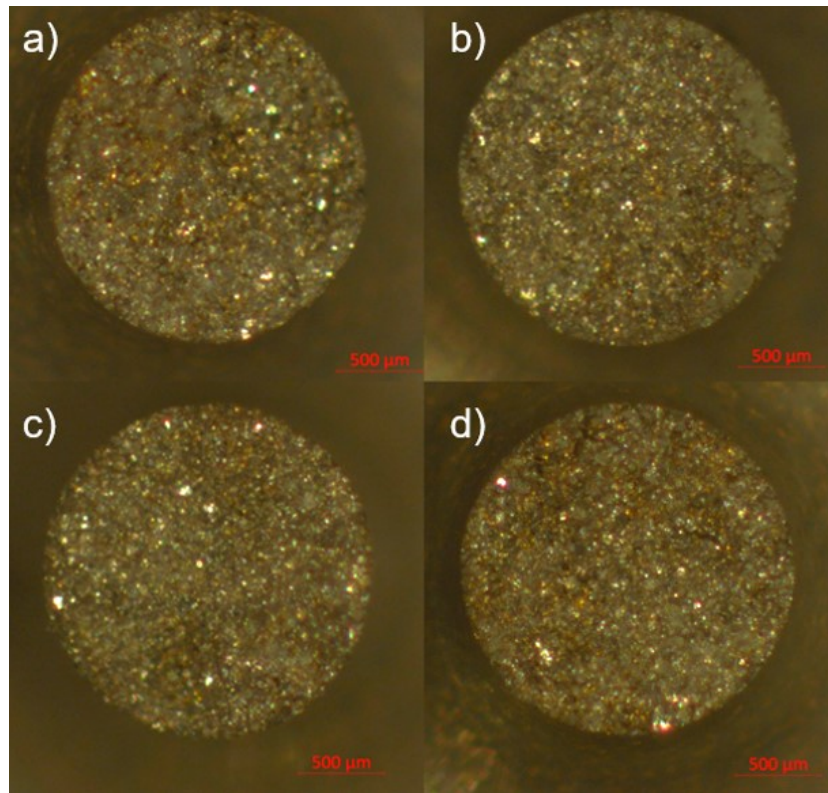


Figure 29: Macroscopic images of Sn 2 sample. MAG: 200x Scale bars: 500 μm .

In [Fig. 29](#) one can see that all of the specimens have flat fracture surfaces with a low degree of topography. Some pores can also be seen in a) and d).

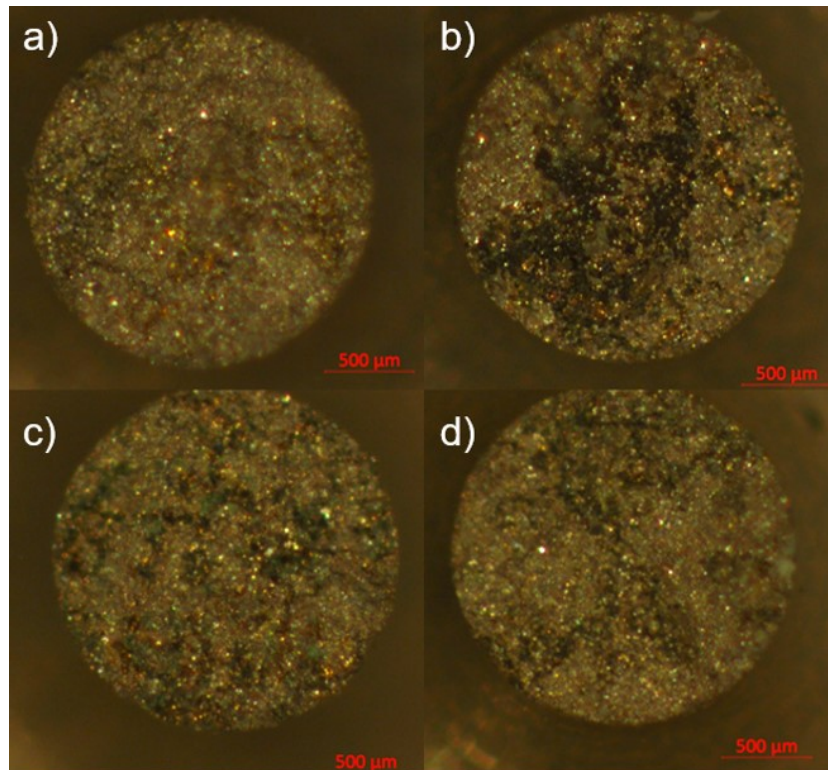


Figure 30: Macroscopic images of Sn 13 sample. MAG: 200x Scale bars: 500 μm .

As seen in [Fig. 30](#), the pores more predominant for the Sn 13 sample compared to the Sn 2 sample. Omitting the topography related to the pores, the fracture surfaces are flat similar to the Sn 2 specimens.

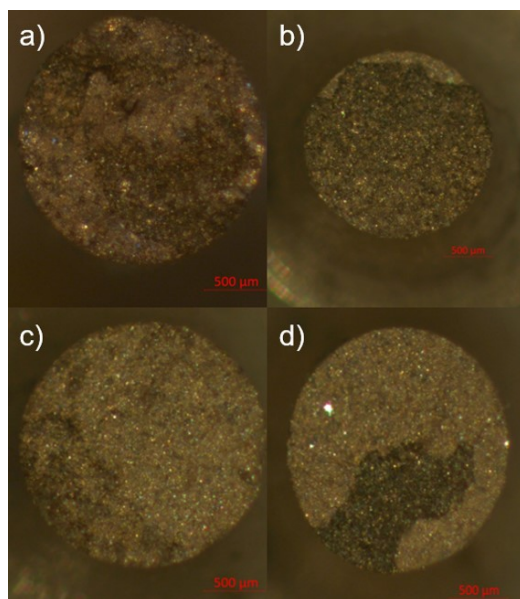


Figure 31: Macroscopic images of Ni 1 sample. MAG: 200x Scale bars: 500 μm .

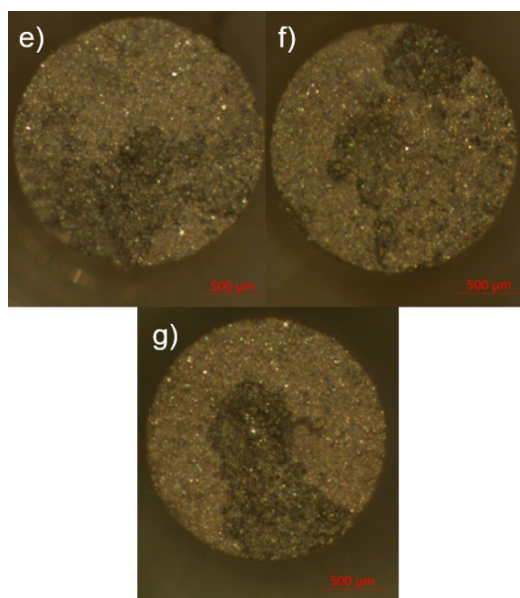


Figure 31: Macroscopic images of Ni 1 sample. MAG: 200x Scale bars: 500 μm .

Fig. 31 show the fracture area of all of the seven tensile test specimens tested for the Ni 1 sample. Compared with the other two samples, the Ni 1 sample show a larger amount of topographical features.

4.6 Computerized Tomography (CT)

The CT scan results before and after tensile testing are shown in Fig. 32 and Fig. 33 respectively.

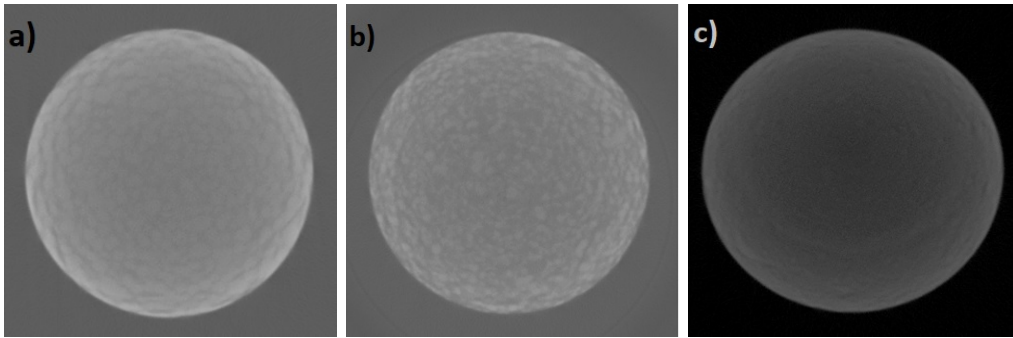


Figure 32: CT of the samples before tensile testing for samples a) Sn 2, b) Sn 13 and c) Ni 1. The lightest phase seen is tungsten phase, while the darker network phase is the Cu-Sn phase. Pores in the material is also seen as dark phase, and is hard to distinguish from the Cu-Sn phase.

To see the development of the topography of the fracture area, CT images were put together in videos. A link to the videos can be found in Appendix A. One snapshot from each of the videos are seen in Fig. 33.

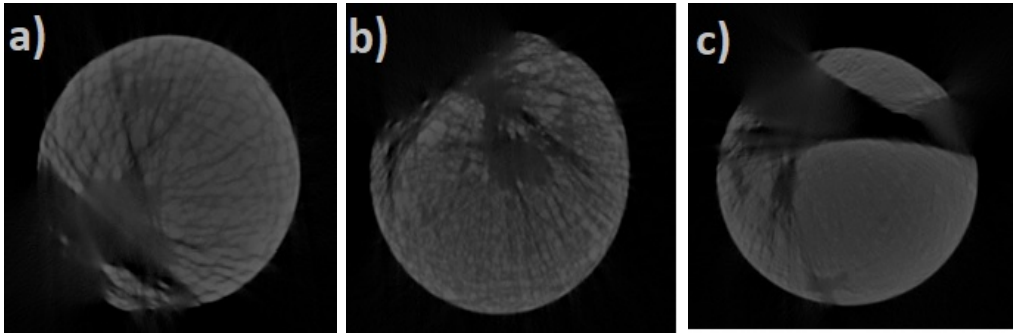


Figure 33: CT of the fracture area in samples after tensile testing for samples a) Sn 2, b) Sn 13 and c) Ni 1. The lightest phase seen is tungsten phase, while the darker network phase is the Cu-Sn phase. Pores in the material is also seen as dark phase, and is hard to distinguish from the Cu-Sn phase.

4.7 Optical Microscope (OM)

The OM images were taken of one specimen for each of the samples. Pictures were taken with 25x, 50x, 100x, 200x, 500x and 1000x magnification.

4.7.1 Unaffected zone

One specimen for each sample were analysed from the bottom of the tensile test specimen to examine the microstructure resulting from the infiltration, unaffected by the tensile testing. These analyses are therefore termed as examining the unaffected zone.

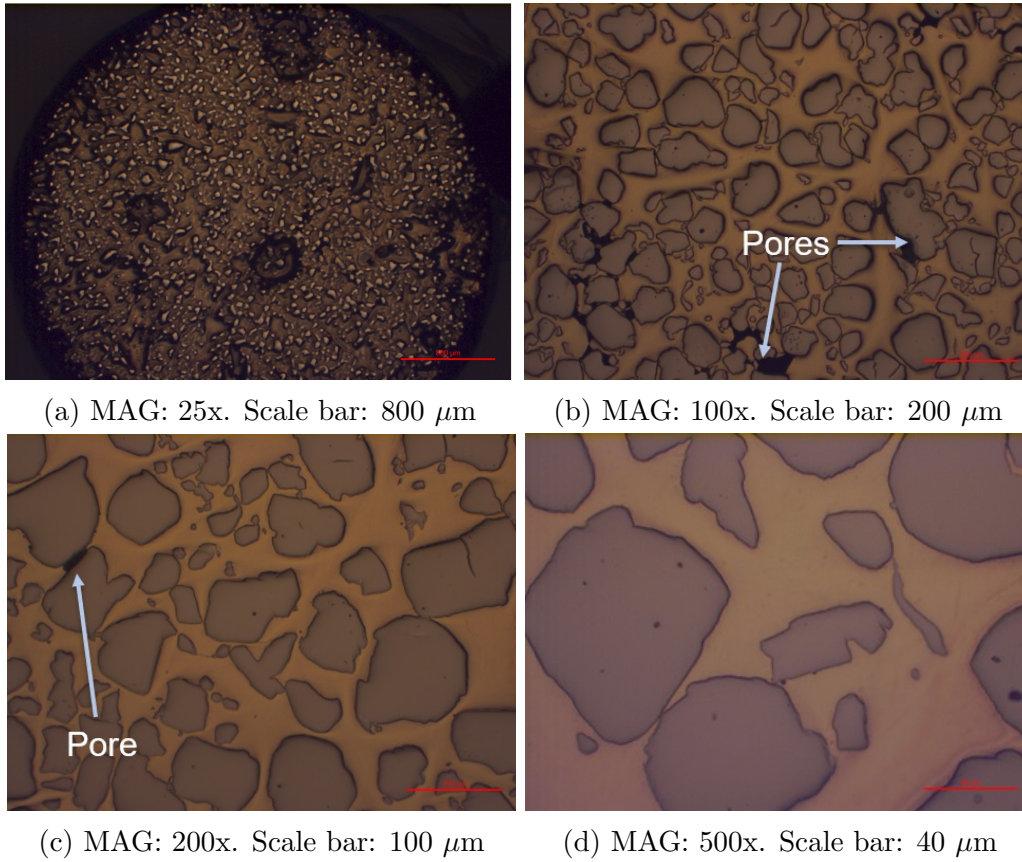


Figure 34: OM of the unaffected zone of the Sn 2 sample.

In [Fig. 34](#) the microstructure is characterized by tungsten grains surrounded by the Cu-Sn bulk phase. Especially noticeable is the high amounts of pores, which in general are large.

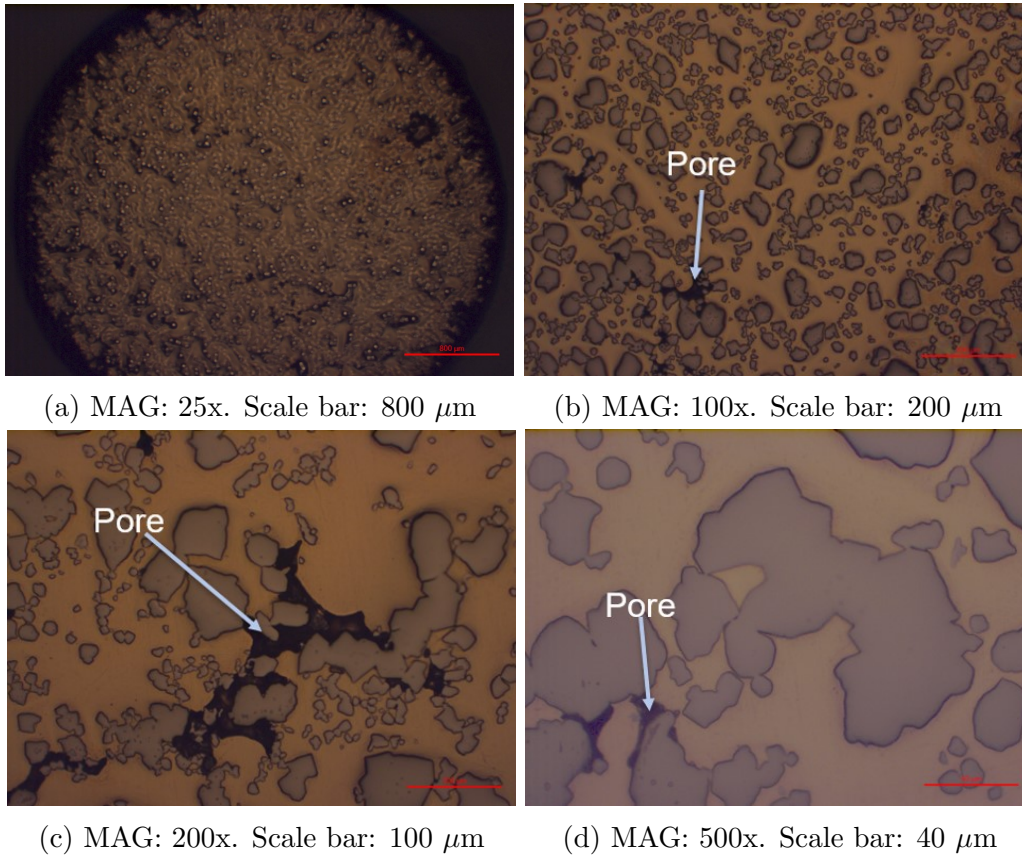


Figure 35: OM of the unaffected zone of the Sn 13 sample.

In [Fig. 35](#) the microstructure is characterized by tungsten grains surrounded by the Cu-Sn bulk phase. In the sample there is a larger grain size distribution and pores are more evenly distributed throughout the material, compared to the Sn 2 sample. Some of the pores are also very large.

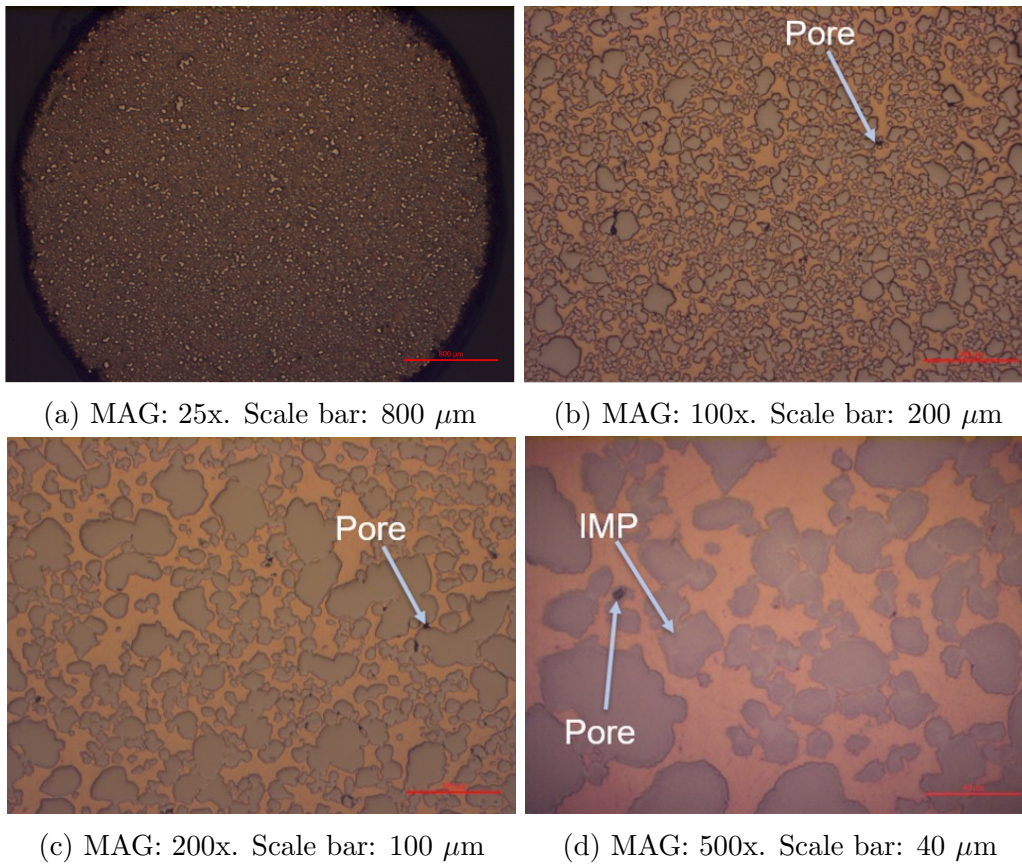


Figure 36: OM of the unaffected zone of the Ni 1 sample.

In Fig. 36 the microstructure is characterized by tungsten grains surrounded by the Cu bulk phase. For this sample a much more homogeneous microstructure is seen. There are still a large amounts of pores in the material, although much smaller than pores than for Sn 2 and Sn 13 samples. As seen in (d), large magnification reveals the formation of intermetallic phase (IMP) growing in between tungsten grains.

4.7.2 Fracture area

Four modes of fracture were identified by Prabhu et al. for tungsten heavy alloys [15]: Transgranular failure, secondary cracks, decohesion along tungsten-matrix interface and intergranular failure. The first two modes are in correspondence with brittle material behaviour, while the latter two are char-

acteristic ductile material behaviour. Intergranular failure leaves W-grain intact.

One of each of the samples were analysed in the fracture area to examine the microstructure to determine the modes of fracture present in the samples. (see Fig. 18 in section 3.1)

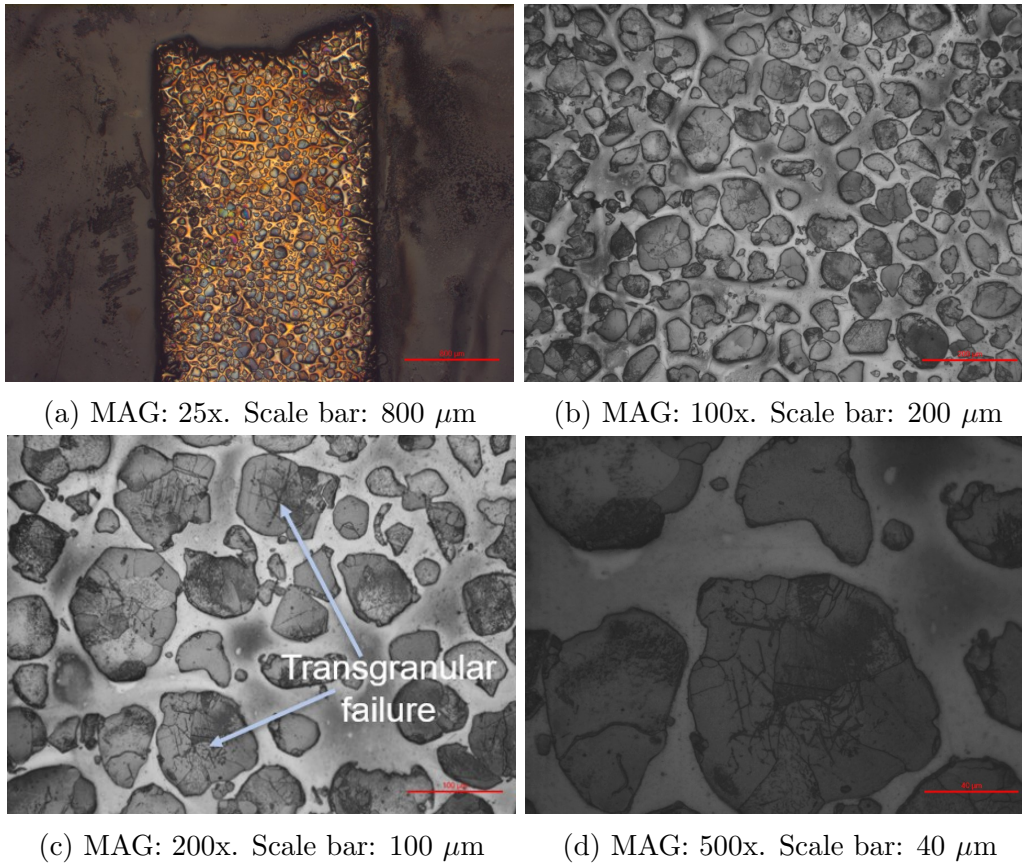


Figure 37: OM of the fracture area of the Sn 2 sample. Transgranular failure

To be able to see the microcracks formed by the transgranular failure better, the Sn 2 sample was examined with higher magnification as featured in Fig. 38. The cracks formed along specific crystallographic planes.

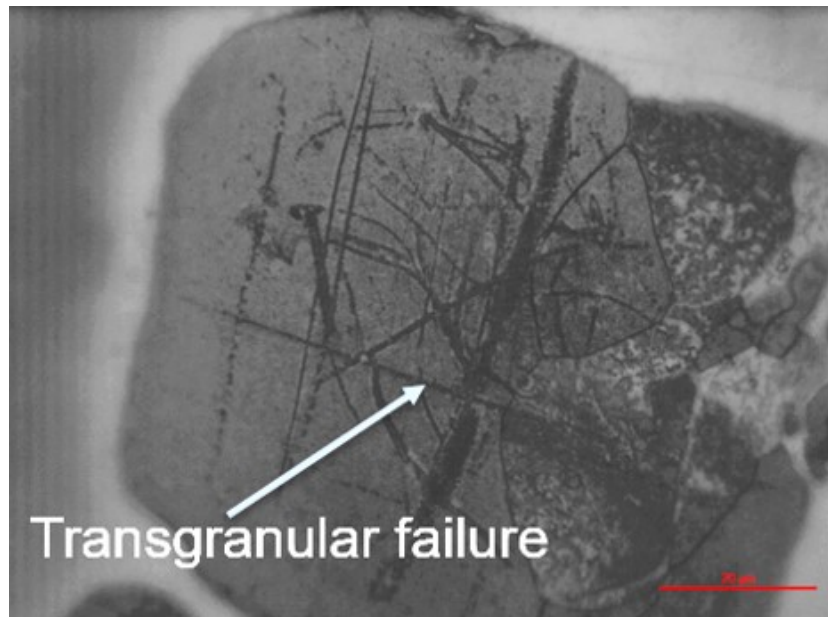


Figure 38: OM of the fracture area of the Sn 2 sample with higher magnification to highlight the transgranular failure of tungsten grains. MAG: 1000x. Scale bar: 20 μm

Unlike the Sn 2 sample, the Sn 13 sample show no clear signs of transgranular failure. As seen in [Fig. 39](#) the tungsten grains are fully intact.

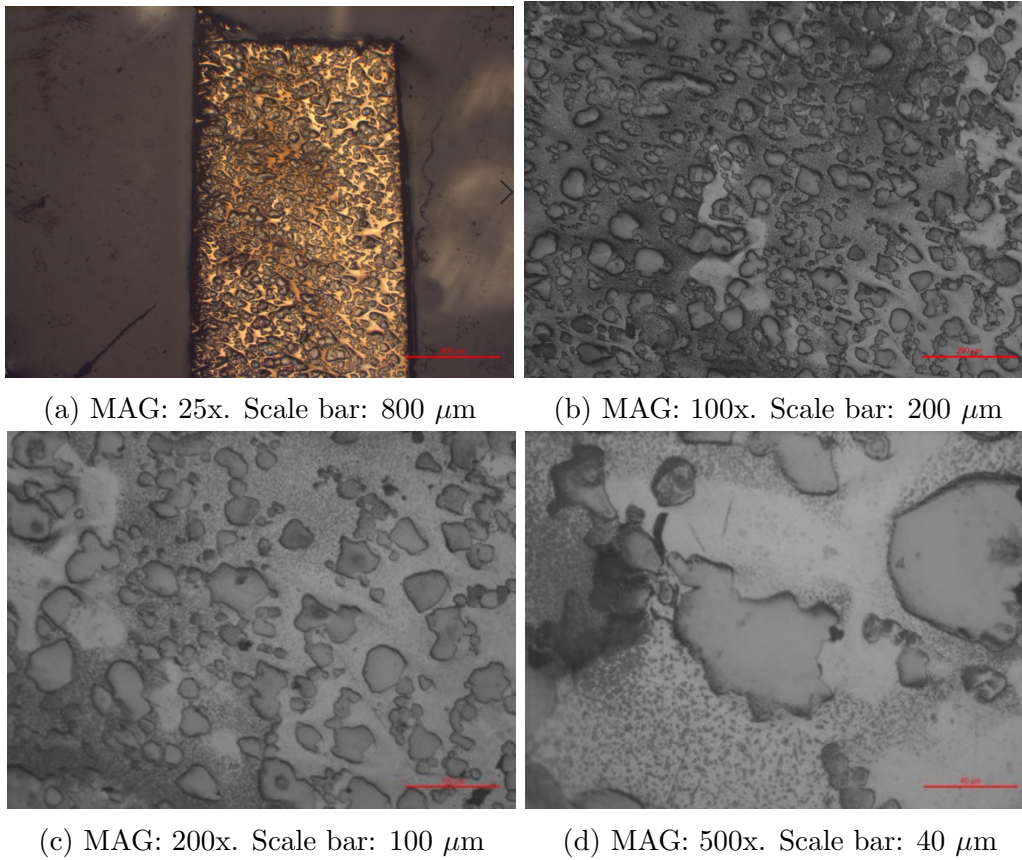


Figure 39: OM of the fracture area of the Sn 13 sample.

The Ni 1 sample show a combination of some transgranular fracture, while other tungsten grains are kept intact. It is therefore a more mixed mode of fractures seen. [Fig. 40](#)

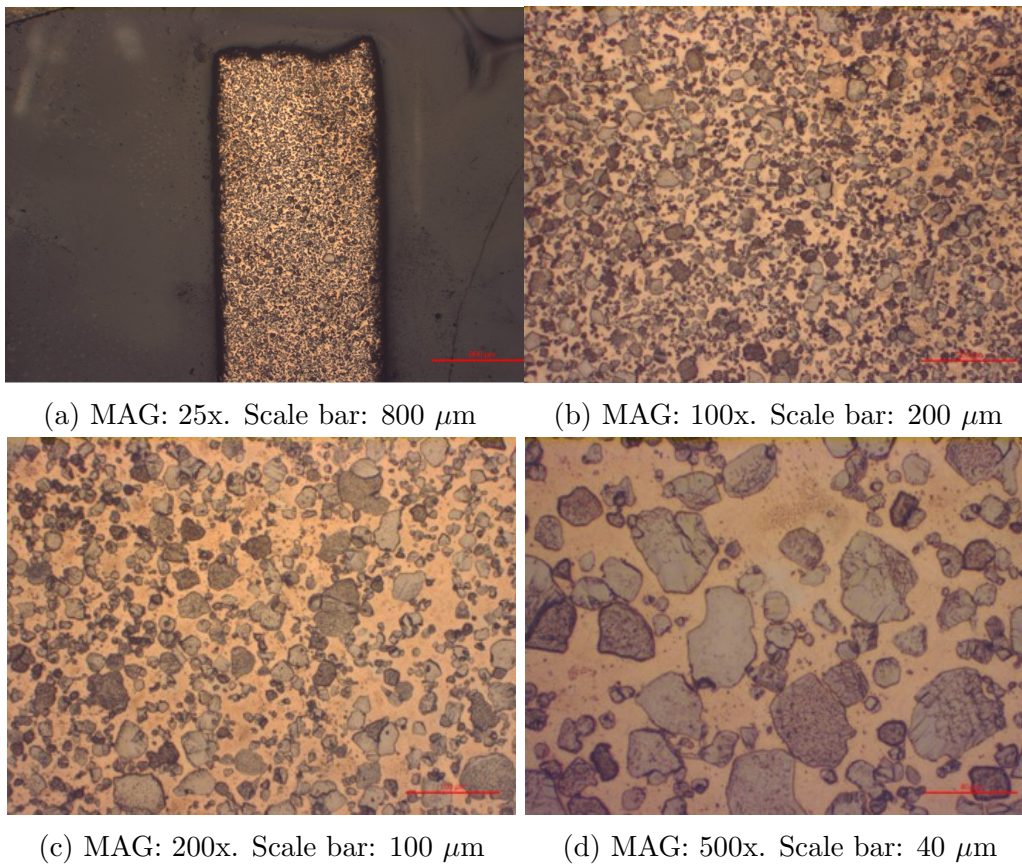


Figure 40: OM of the fracture area of the Ni 1 sample.

4.8 Scanning Electron Microscope (SEM)

SEM images were taken of one specimen from each of the samples in addition to some chosen specimens of the Ni 1 sample.

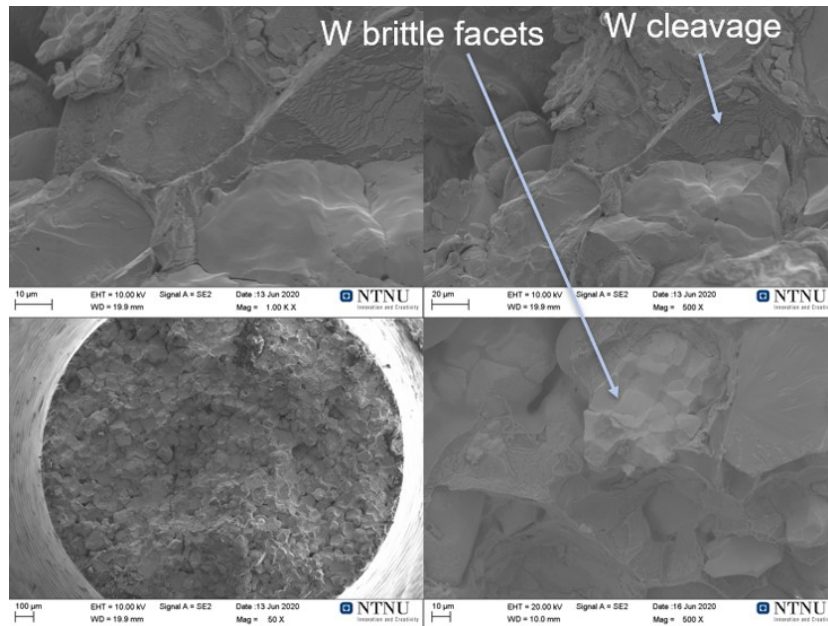


Figure 41: SEM images of the Sn 2 sample.

In Fig. 41 one can see the brittle W facets and W cleavage in the microstructure of the fracture area.

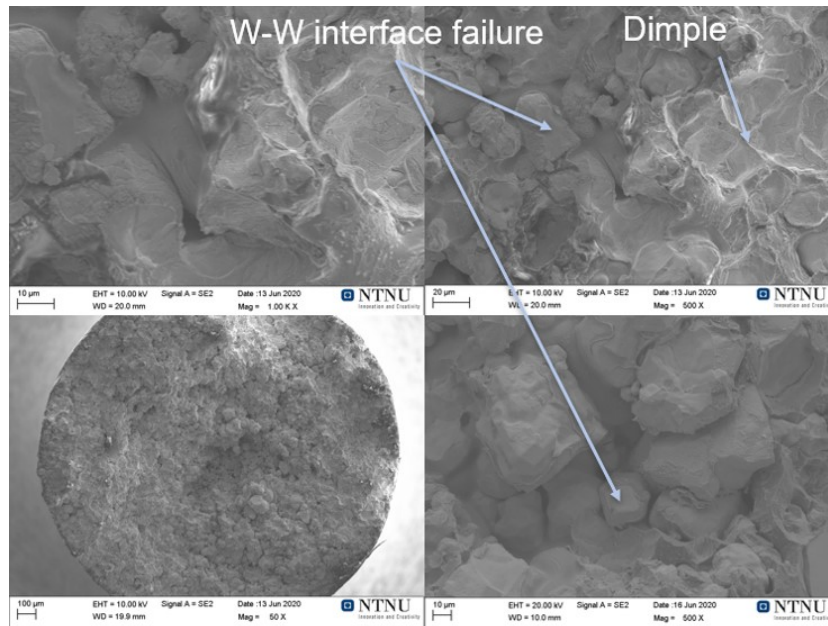


Figure 42: SEM images of the Sn 13 sample.

In Fig. 42 one can see both the W-W interface failure and the dimple fracture structure.

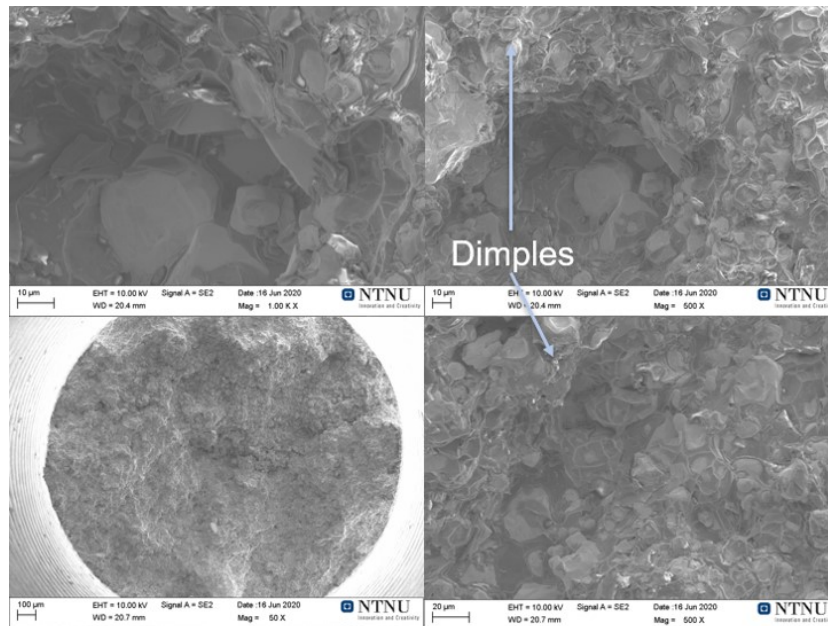


Figure 43: SEM images of the Ni 1 sample.

In [Fig. 43](#) one can see the dimple fracture structure throughout all of the specimen, and also some river pattern is present. To get a closer view of the river pattern in the Ni 1 sample, a zoomed image is shown in [Fig. 44](#).

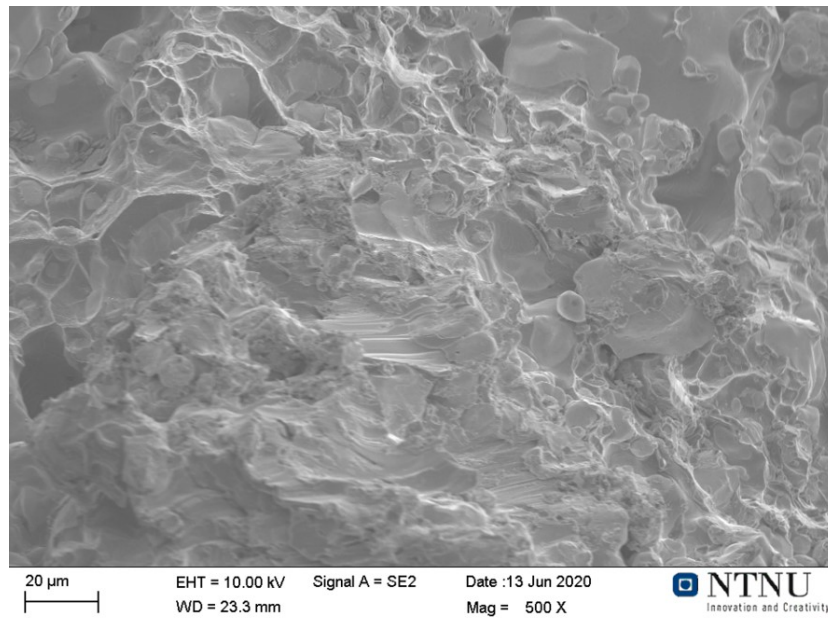


Figure 44: SEM images of the Ni 1 sample showing river pattern.

4.9 Energy-Dispersive X-ray Spectroscopy (EDS)

One EDS scanning were conducted. The follow figures, the results are given.

4.9.1 Point scan

Point scan were used to get quantitative results for the composition of the phases.

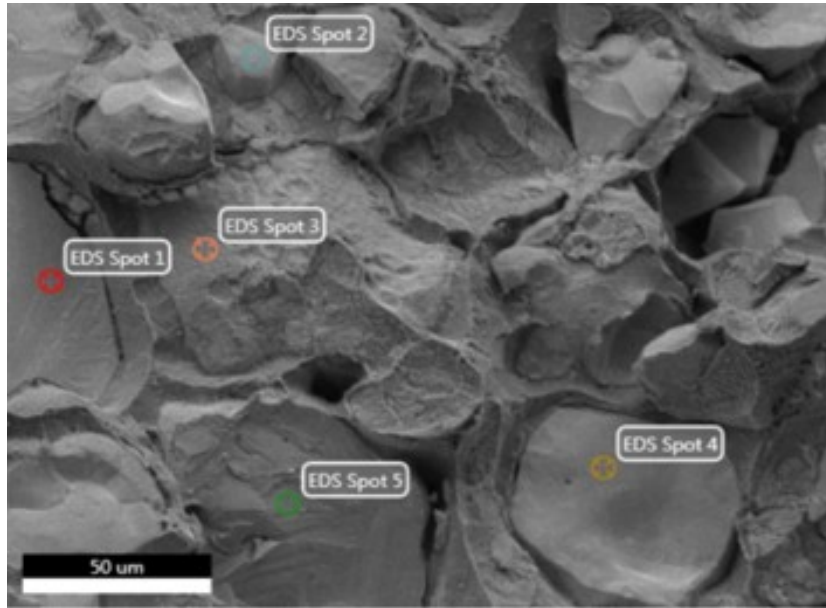


Figure 45: EDS Point scan of Sn2 sample.

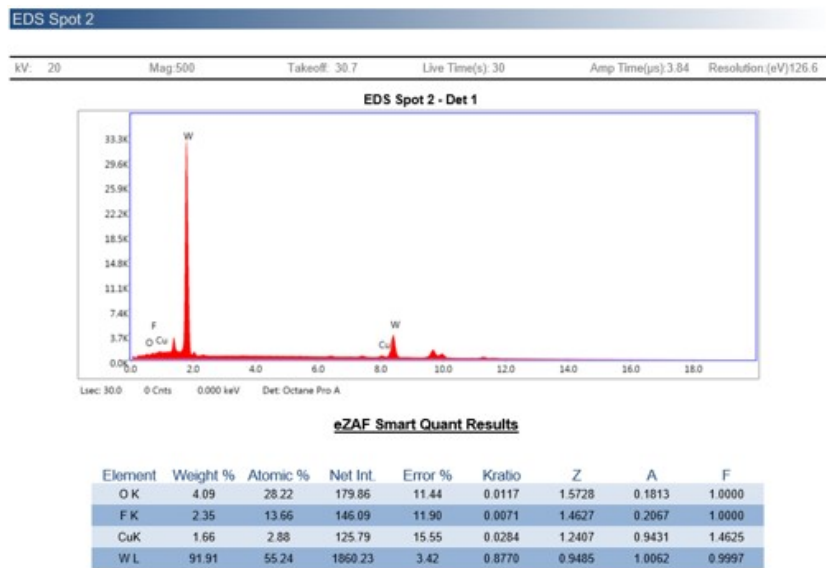


Figure 45: EDS Point scan of EDS Spot 2 of Sn 2 sample.

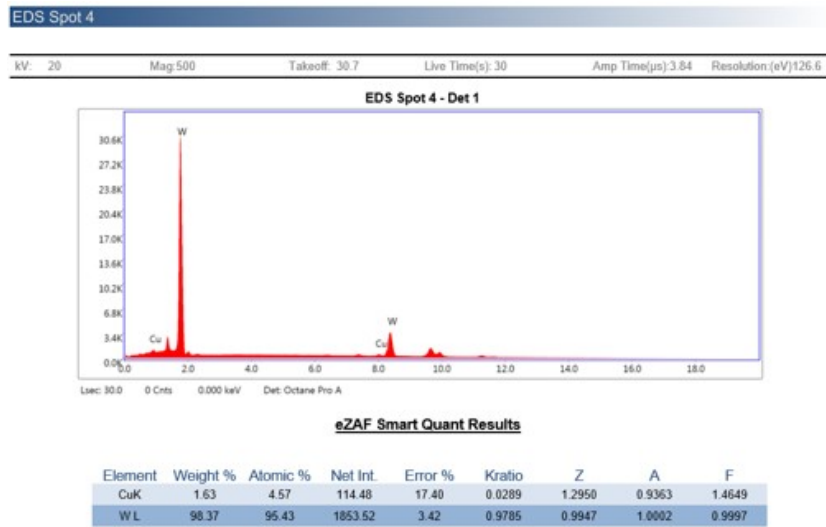


Figure 45: EDS Point scan of EDS Spot 4 of Sn 2 sample.

In Fig. 45 the quantitative results of the EDS Spot 2 and EDS Spot 4 are shown. Notice the high amount of W measured in both points.

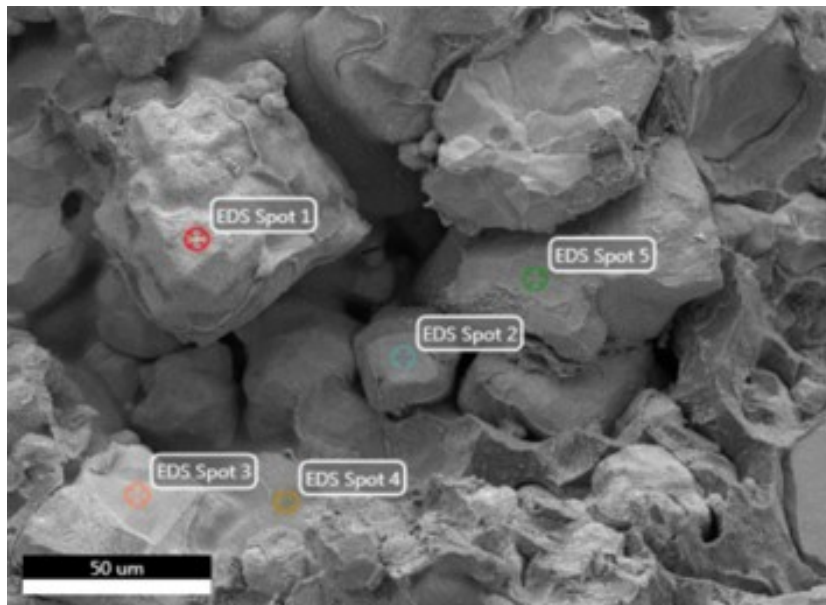


Figure 46: EDS Point scan of Sn 13 sample.

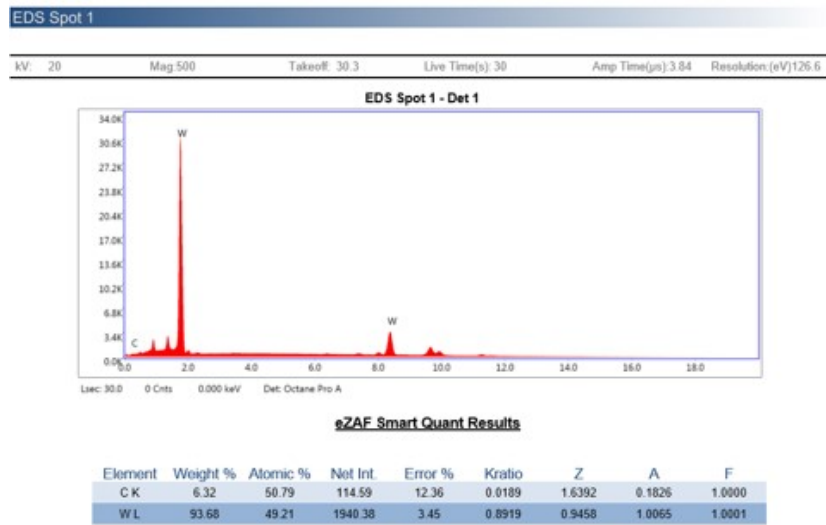


Figure 46: EDS Point scan of Sn 13 sample.

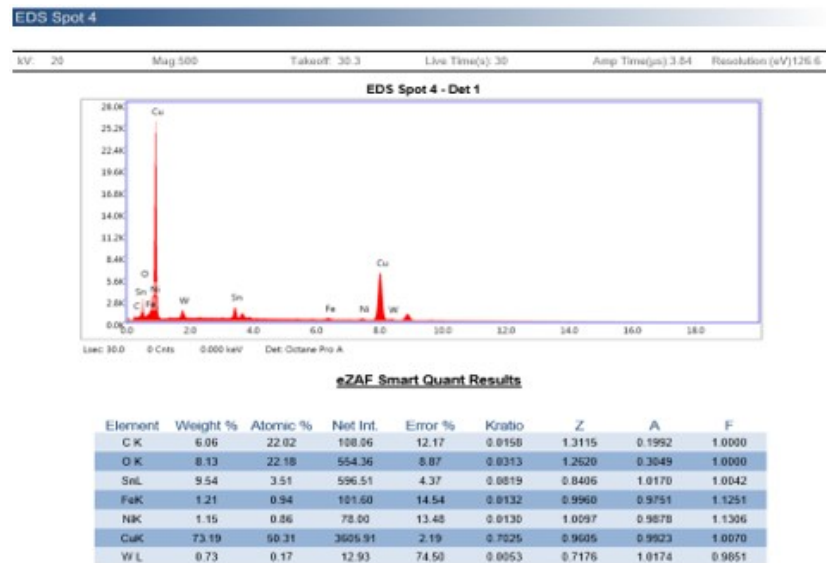


Figure 46: EDS Point scan of Sn 13 sample.

In Fig. 46 the quantitative results of the EDS Spot 1 and EDS Spot 4 are shown. Notice the high amount of W in EDS Spot 1 and the high amount of Cu and Sn in EDS Spot 4.

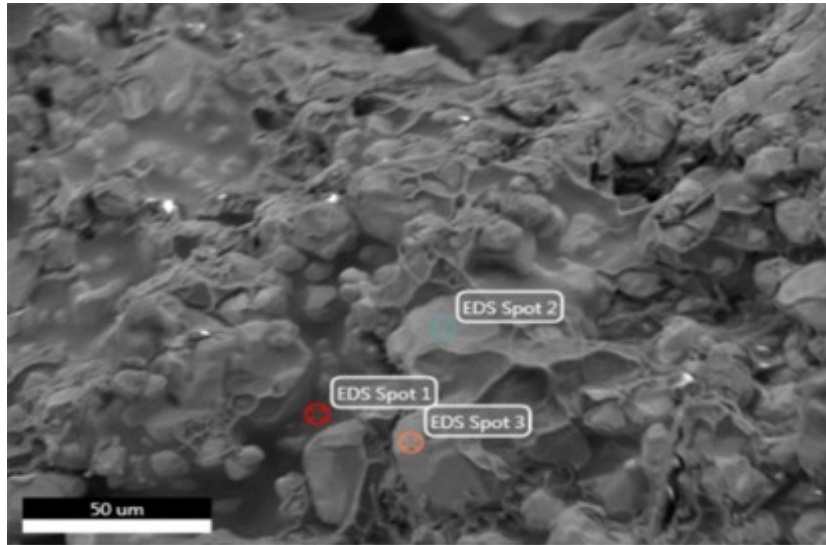


Figure 47: EDS Point scan of Ni 1 sample.

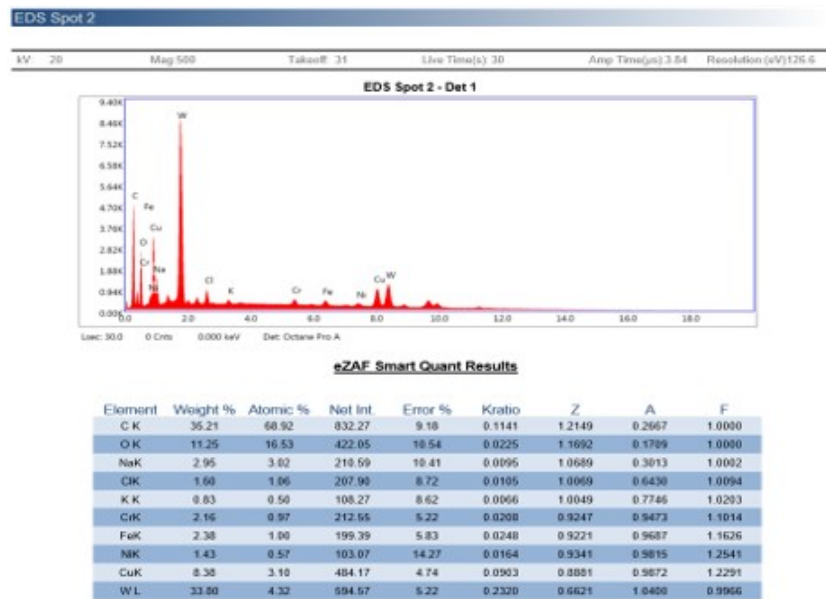


Figure 47: EDS Point scan of Ni 1 sample.

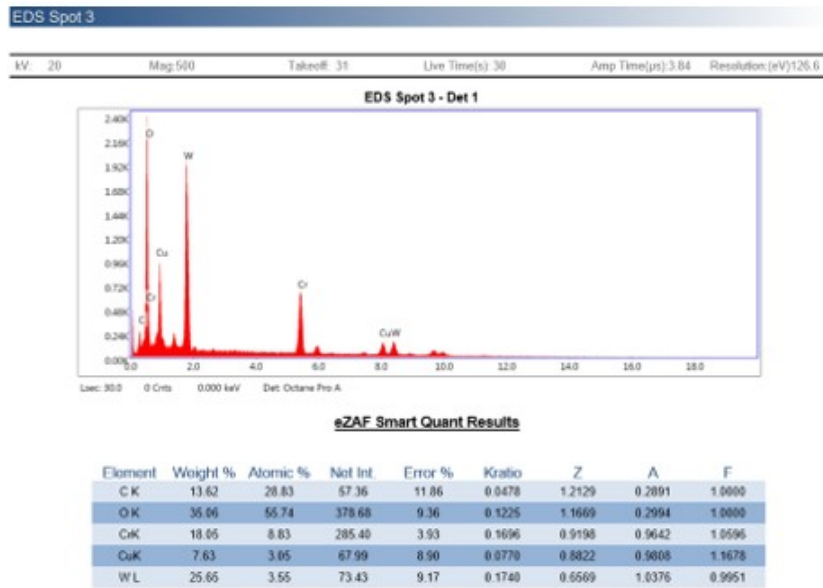


Figure 47: EDS Point scan of Ni 1 sample.

In Fig. 47 the quantitative results of the EDS Spot 2 and EDS Spot 3 are shown. Notice the wide range of elements detected for both EDS Spots, and the high amount of Cr and O for the EDS Spot 3.

4.9.2 Mapping

The EDS Mapping were used to get an overview of where the different elements are in the microstructure. The dark areas are pores or areas shaded by topography. For Sn and W the L_{α} -radiation were detected, due to the high atomic number, Z. [9]

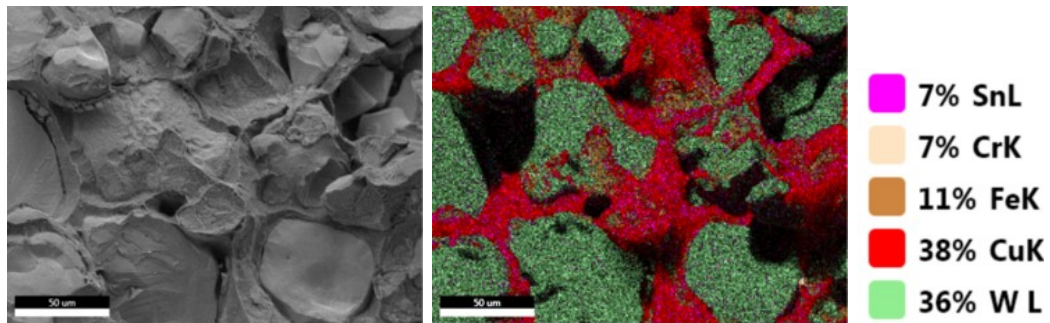


Figure 48: EDS Mapping of Sn 2 sample.

As seen in Fig. 48-49, the W and Cu phases cover different areas of the microstructure, Sn and Fe are present throughout the material, but more predominantly in the Cu phase and the W phase respectively.

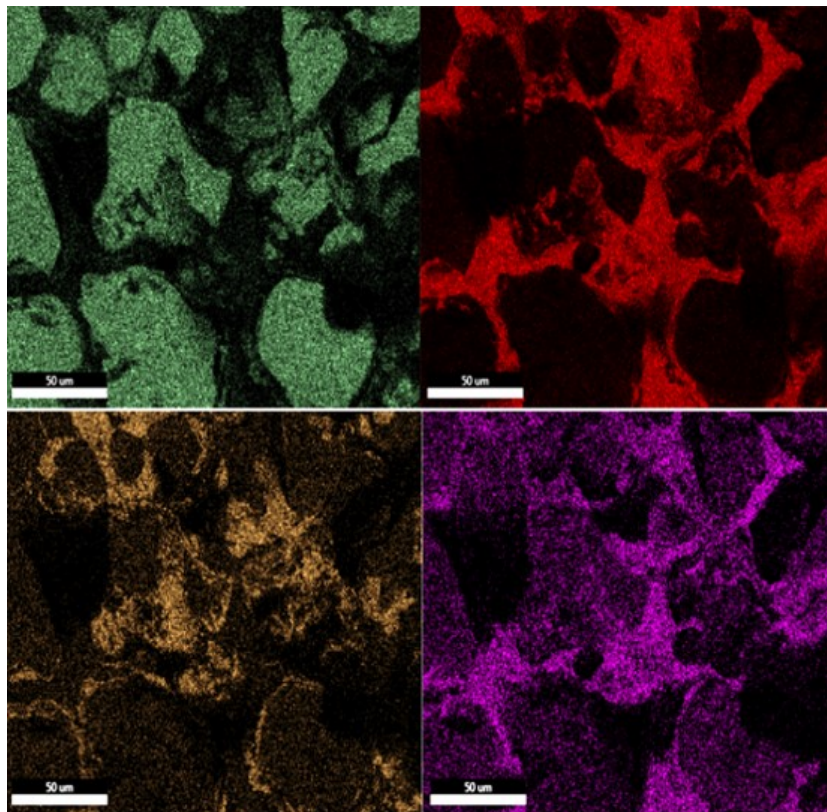


Figure 49: EDS Mapping of Sn 2 sample showing the different elements

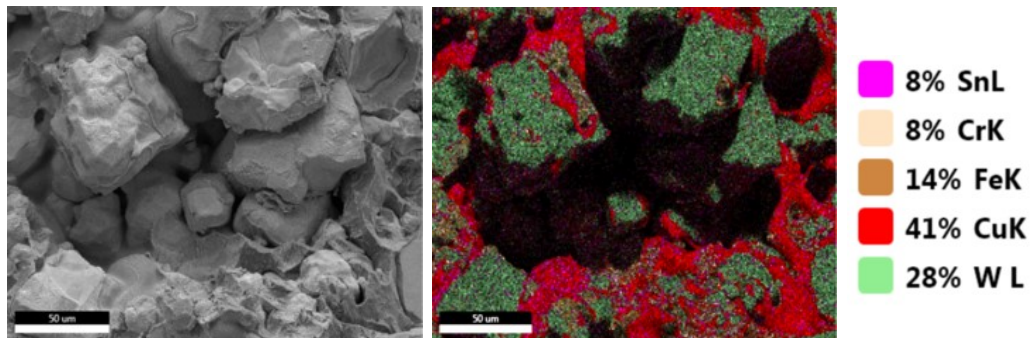


Figure 50: EDS Mapping of Sn 13 sample.

For the Sn 13 sample, the case is the same as for the Sn 2 sample, with W and Cu covering different areas and Sn and Fe present throughout the material as seen in [Fig. 50-51](#).

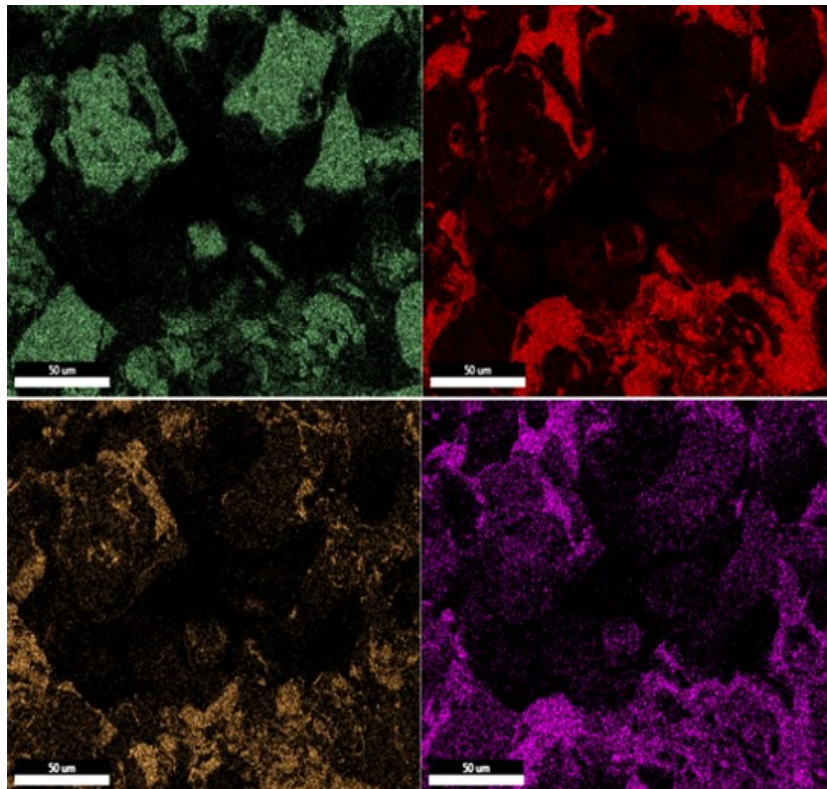


Figure 51: EDS Mapping of Sn 13 sample showing the different elements

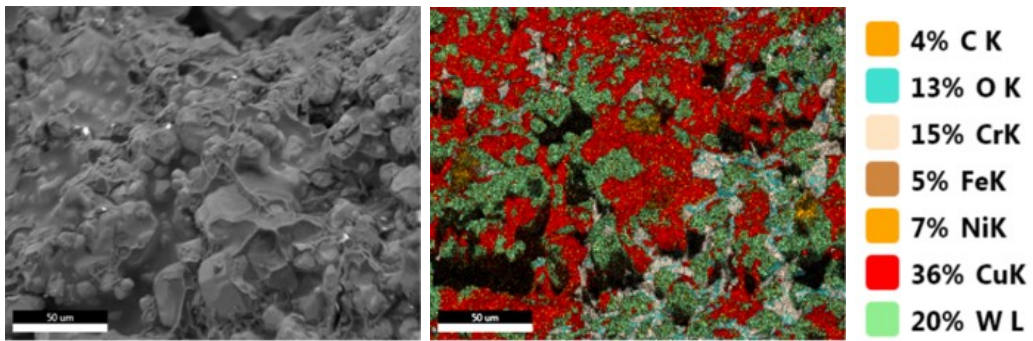


Figure 52: EDS Mapping of Ni 1 sample.

As seen in [Fig. 52-53](#) the W and Cu show the same trend as for the other two samples, but the Ni on the other hand is present throughout the whole material. Cr and O cover specific areas not related with the other phases.

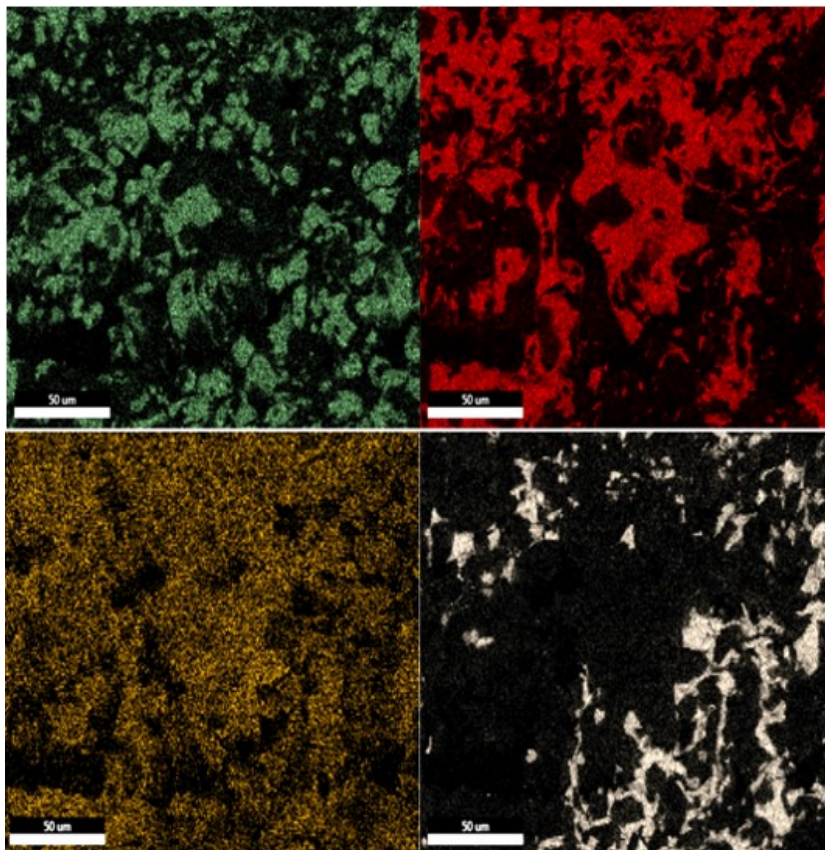


Figure 53: EDS Mapping of Ni 1 sample showing the different elements

5 Discussion

In this section the results presented in section 4 will be compared with the material specifications and be discussed highlighting possible improvements by using the theory. Firstly the material properties will be discussed, secondly the microstructure, thirdly the crucible material impact on the infiltrated product and lastly the recycling and recovery of tungsten from W-Cu composites will be discussed.

5.1 Material properties

In this section the results relating to the material properties of the composite is discussed. Firstly the density measurements will be discussed, followed by comparing the tensile tests and the relating measurements with the material specifications. The material specifications being E-modulus above 190 GPa, YS above 200 MPa and A_{tot} above 5%. (see section 1.2).

5.1.1 Density

The density measurements conducted on tensile test specimens are quite inaccurate, as can be especially seen by the Sn 2 sample having larger density measured than its theoretical density. This is due to the small volumes measured. The variation of ± 0.01 mL changes the density measured with ± 0.5 g/cm³. The 10 mL measuring cylinder used has marked every 0.2 mL, and the accuracy in range of 0.01 mL is therefore hard to distinguish using the naked eye. Density measurements should therefore be taken on larger specimens, to give more accurate results. The densities measured at Sandvik after infiltration (before milling to tensile test specimens) gives therefore the most accurate results.

Based on the densities measured at Sandvik, sample Sn 2 and Sn 13 show fully densification with 99.03% and 99.27% relative density respectively. The density measured at Sandvik for the Ni 1 sample, were not accessed. By using the average density measured of the tensile test specimens, a relative density of 93.05% was measured. The relative densities measured based on tensile test specimens for the Sn 2 and Sn 13 samples were 103.38% and 90.85% respectively (see Table 2 in section 4.1). The Ni 1 sample results had the largest standard deviation with ± 1.47 g/cm³. As seen in the OM results, the Ni 1 sample showed a more homogeneous microstructure compared with the

other two samples. Given that the two bronze samples show, based on density measured at Sandvik, almost fully densification, it is probable to assume the Ni 1 sample have a similar high relative density. The results showing fully dense composites is a clear statement of a successful infiltration process. The relative densities were calculated using equation (9) from section 4.1.

5.1.2 Tensile tests

As seen in the tensile curves in section 4.2 and in Table 3, there is a large distribution in the results. The problem with using a composite material, is the large dependence of volume fraction of the phases on the mechanical properties. To be able to get more reproducible results, a more evenly distribution of phases and a more homogeneous microstructure is required.

In Fig. 54, the best tensile curve for each sample is put together. It is clear to see that the Ni 1 sample have better mechanical properties with the highest elastic modulus, the highest yield strength and the longest elongation. The tensile curve for the Ni 1.4 tensile test specimen shows the desired shape, with steep increase in stress in the elastic region, and relative long elongation in the plastic region. The specimen fulfills two out of three material specifications, but lacking the high resistance to elastic deformation required for the application.

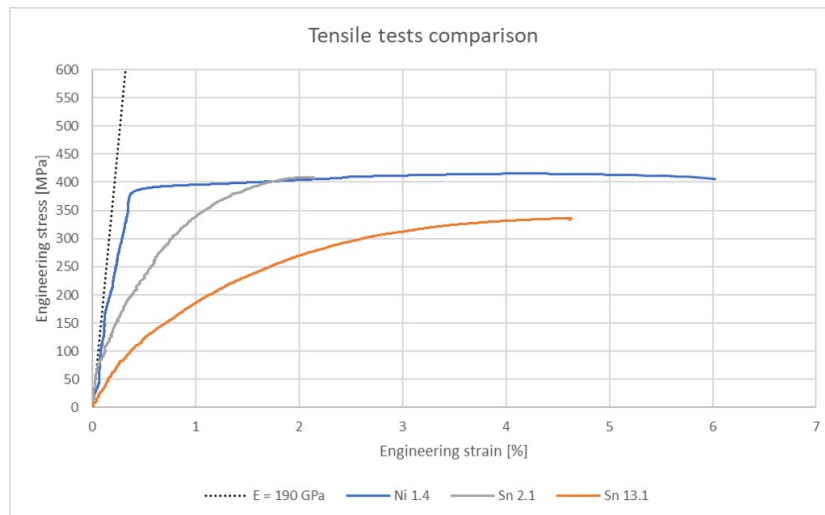


Figure 54: Selected tensile curves for each of the samples.

5.1.3 Reduction of area (q)

For engineering tensile curves the stress decreases beyond the ultimate tensile strength (UTS). This is due to the phenomenon known as necking, where the cross sectional area is reduced. The larger the reduction of area, the more ductile the material is. The distinction between brittle and ductile material lies around 5% total elongation [4].

As seen in the table in section 4.3 (see Fig. 27), the percentage reduction in area is for most of the specimens zero or in general show small values. The initial area were assumed to be milled equally for all specimens after the specification, although the diameter were milled to 1.95 mm (recall specified diameter of 2.0 mm (see Fig. 20). The negative values for q comes from a larger diameter measured after testing, compared with milled specification. In practicality the negative values are to be treated equivalently as the zero values. q should always be unity or larger for a tensile test, due to the conservation of volume during testing, the increase in length requires similar decrease in cross-sectional area [4].

The area reduction results agree upon the tensile test results (tensile curves), in the way that the Ni 1 sample shows more ductility than the two bronze samples. Although contradictory to the elongation results, specimen Ni 1,4 (which shows the largest elongation, the only to attain the criteria) measured no reduction in area. It can be concluded that the composite is brittle, but the inclusion of Ni makes the material more ductile. The NyDeMa project is therefore on the right path towards fulfilling the material specification.

5.1.4 Elastic Modulus

The rule-of-mixtures depicts the elastic modulus for tungsten-copper composites based on volume fraction and elastic modulus of the particulate and matrix phases [4]. Tungsten is the particulate phase and copper is the matrix phase for W-Cu composite. An upper and a lower limit gives the range of elastic modulus to be expected.

Values for modulus of elasticity and density were accessed from *Materials Science and Engineering SI Version* [4]. At room-temperature the modulus of elasticity is 407, 110 and 207 GPa for tungsten, copper and nickel respectively. At 20 °C the density is 19.3, 8.94 and 8.90 g/cm³ respectively. In the calculations, the density value for copper were used for the matrix phase, as the dissimilarity with nickel were deemed negligible. The rule-of-mixtures

equations (3) and (4) in section 2.4 were used to calculate the necessary volume fraction to fulfill the elastic modulus requirement. The results are plotted in Fig. 55. The horizontal line corresponds to $E = 190$ GPa.

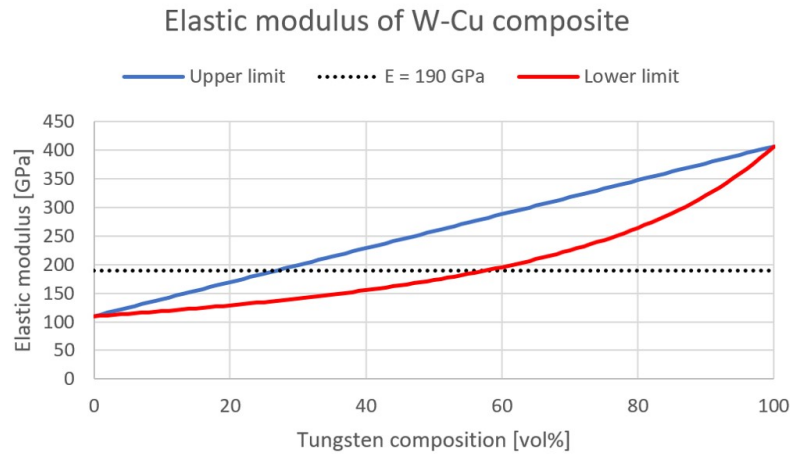


Figure 55: Elastic modulus of W-Cu composite as a function of composition.

The material specification of Young's modulus of ≥ 190 GPa is for most of the tensile tests not fulfilled. As seen in Fig. 55, to confidently achieve a larger elastic modulus than 190 GPa, a tungsten volume fraction of at least 58 vol% is needed. For the samples tested, the volume fraction of tungsten were 60, 38 and 45 vol% for the Sn 2, Sn 13 and Ni 1 samples respectively. This would explain why this material specification is not fulfilled for the latter two samples. For the Sn 2 sample the results are much lower than anticipated by the theoretical volume fraction tungsten. This is probably due to high amount of pores in the material.

In Fig. 56 the theoretical density of the composite is plotted against composition. The two red vertical lines corresponds to the intersection between upper and lower limit for the elasticity modulus with the $E = 190$ GPa line, left and right vertical line respectively. The corresponding values for tungsten composition are 27 and 58 vol% for the lower and upper limit respectively. Therefore at least 27 vol% is needed to fulfill the material specification, and above 58 vol% to ensure it is fulfilled.

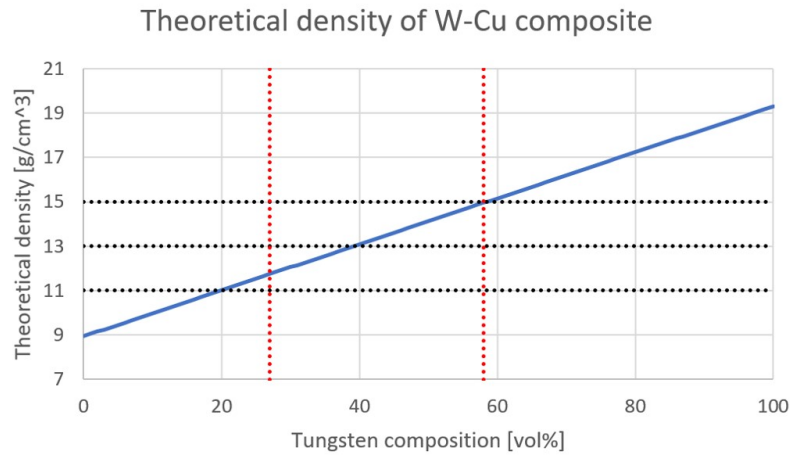


Figure 56: Theoretical density of W-Cu composite as a function of composition. The blue line shows the theoretical density based on volume fraction of tungsten.

In Fig. 56 the black horizontal lines gives the two density ranges of products covered by the application. The higher density products in the range 13-15 g/cm³ will only at the higher end of the range achieve the requirement confidently. For the lower range of 11-13 g/cm³, components will not confidently fulfill the requirement throughout the range. Therefore W-Cu composites are better suited for the higher density range for the given application. The Ni addition enhance the modulus of elasticity (recall the elastic modulus of Ni is 207 GPa), while the modulus is reduced with increased porosity in the material. The effect of the latter two will cancel each other out to some degree, but to reliably achieve the requirement, a larger theoretical density should be aimed for. This due to the porosity being a parameter which is harder to control.

5.1.5 Material specification

The combination of the three criteria specified for the application combined with the high density, requires the material to combine both high strength and ductility, while the available elements are limited to be used for attaining the density requirement. W-Cu show good potential for the use.

The tensile test results show that the elastic modulus criterion is not fulfilled for any of the three samples. The Ni 1 sample shows the highest E-modulus with 98.12 GPa, but have also the largest standard deviation with 64.72 GPa. Even though the Ni 1 sample shows the best potential to this regard, the large discrepancies in the results make it not reliable in application.

For the yield strength (YS) all three samples attain the criterion, with both sample Sn 2 and Ni 1 fulfilling it with a good margin. There are some deviations in the results, but at a much lower magnitude compared with the other two properties looked at. The YS is an important property especially for a brittle material, which will not deform plastically before initiating fracture. Sudden applied large stresses could therefore cause severe damage. The good margin above the YS criterion showed by the Sn 2 and Ni 1 samples are therefore desired.

The elongation increases remarkably from the bronze samples Sn 2 and Sn 13 to the nickel sample Ni 1. Also for this property, the Ni 1 samples shows the largest value with 2.61% and the largest standard deviation with 1.99%. None of the samples fullfill the criterion, and the large variation in the results and with only one of the specimens tested reaching the desired elongation, makes the composites not reliable in application.

5.1.6 Hardness

For the hardness tests, the load were chosen to give the indent size best fitting with the measuring software. For the Sn 2 sample in the unaffected zone, the large particle size of the phases allowed for the indent to measure the two phases of the composite separately. The large spread in the data, for the Sn 2 sample in the unaffected zone, is due to half the measurements were taken of the hard tungsten phase, while the other half were of the soft copper phase. (see [Fig. 28](#) in section 4.4) For the other tests, the indent covered parts of both phases, giving more deformed indents (deviation from the square shape) and resulting in values in between what would be expected for the phases separately. The highest hardness was for both zones measured for the Sn 2 sample, which is probably due to it having the highest amount of tungsten content. The hardness results would have larger accuracy by using a smaller load, giving smaller indents, and are therefore recommended for further measurements.

5.1.7 Macroscope

The macroscope results given in [Fig. 29-31](#) shows the fracture area of specimens, subsequent to tensile testing, seen from above. The Ni 1 samples shows larger range of topography compared with the two bronze samples. The Sn 13 sample have pores extending through the fracture area, while the Sn 2 sample have a relative flat fracture area. The flat fracture area is typical for brittle fracture, while a larger range in the topography are in accordance to ductile fracture, where the material undergoes plastic deformation before initiating fracture.

From the macroscope results it can be concluded that the Ni 1 sample shows a more ductile behavior than the other two samples. The Sn 2 and Sn 13 samples show brittle fracture. The Ni 1 sample therefore shows a more desirable behavior according to fracture area examination.

5.2 Microstructure

In this section the microstructure of the samples will be compared and discussed. The changes at microlevel have a large impact on the macroscopic properties of the composites and microstructure are therefore important to examine.

5.2.1 CT

For the images retrieved from the CT scans, there are a clear distinction between the two phases for the Sn 2 and Sn 13 samples. For the Ni 1 sample on the other hand, the phases are not easily distinguished. As seen in the EDS Mapping results in section 4.9, nickel is present throughout the material, due to being soluble in both tungsten and copper. With nickel and copper having similar atomic numbers (28 and 29 respectively, with tungsten standing out with atomic number 74[3].), they are hard to distinguish in the x-ray signals. Pores in the material are seen as dark areas, but are also hard to distinguish from the dark copper phase.

The images from the CT scans conducted on the fracture area of samples after tensile testing, were assembled together into videos to show how the topography changed throughout the length of the specimen. The videos are linked in appendix A. In the videos it is clear to see that the Ni 1 sample

shows the largest change in topography, which is in accordance with showing a more ductile behavior than the other two samples.

5.2.2 OM

To analyse the microstructure subsequent to infiltration, the bottom of the tensile test specimen were examined unaffected by the tensile testing. The area examined is therefore termed the unaffected zone. The clear distinction in homogeneity of the microstructure from sample Ni 1 showing the best results, to sample Sn 13 showing the worst results with a high grain size distribution. Both the Sn 2 and Sn 13 samples also have larger variation throughout the specimen, with areas containing large pores, seen in the 25x magnification images. (see [Fig. 34-36](#) in section 4.7)

The OM results of the unaffected zone stand opposed to the density measurements, where the latter gives fully densification of composites while the former clearly shows that the tungsten is not entirely infiltrated by copper, due to the large amounts of pores. With the large uncertainty of the density measurements, the OM results should be considered more valid. The infiltration process therefore has room for improvement. The desired increase in homogeneity by improved infiltration will give the resulting composite improved mechanical properties with lower variance.

Based on the literature, the IMP found in the OM images at high magnification of the Ni 1 sample is most probably Ni_4W [5]. The IMP were not detected in the SEM and EDS results. Ni were found in the EDS results throughout the material, but as Ni is soluble in both tungsten and copper, it is difficult to distinguish solid solution and IMPs using the methods applied on a fracture area. For the identification of IMPs, the sample tested should be polished to a flat surface to receive accurate results. By performing line scans, IMPs present will show a distinct change in composition to a specific fraction.

The nature of the IMP determines the effect they have on the microstructure. They can contribute to strengthen the material, or the opposite if they are brittle phases. The nature of the suggested IMP is unknown. Further analyses between different infiltrated W-Cu-Ni composites are needed, to see which parameters effect the formation of these IMPs, and compare the mechanical properties. The infiltration parameters can then be tuned to either enhance or limit the formation according to whether or not it is deemed a favorable constituent in the microstructure.

For the analyses of the fracture area in OM, the three samples can be characterised with sample Sn 2 showing brittle transgranular failure, sample Sn 13 showing tungsten grains intact and sample Ni 1 showing a mix of intact tungsten grains and transgranular failure. The Sn 2 sample is therefore brittle, the Ni 1 sample shows a mixed mode of fracture, while the Sn 13 sample is based on these results unclear. The tungsten grains left intact is the result of a brittle fracture mechanism of tungsten-tungsten grain decohesion, but the results are not as characteristic as for the transgranular failure.

5.2.3 SEM

One SEM images from each of the samples were chosen based on being representative for the fracture modes present in the different samples. The chosen images from Fig. 41-43 are placed together in Fig. 57.

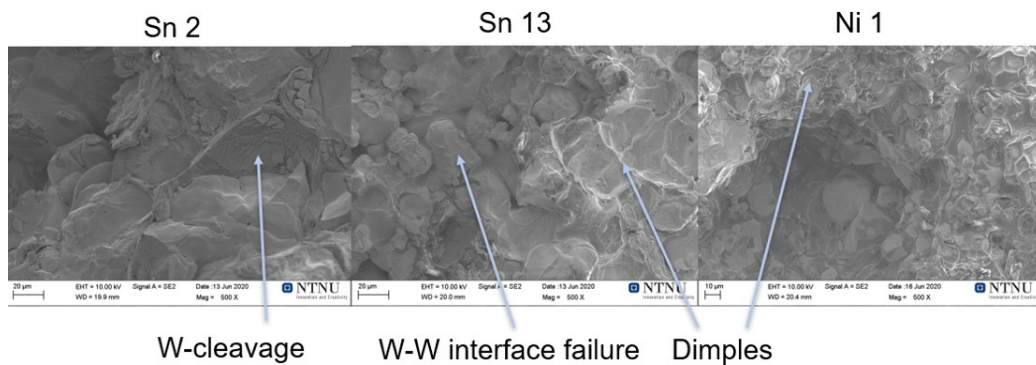


Figure 57: Comparing the SEM images for all samples.

Both the W-cleavage shown for the Sn 2 sample and the W-W interface failure shown for Sn 13 sample, are brittle fracture modes, which are undesired for the given application. The dimple structure seen throughout the Ni 1 sample, and also present in the Sn 13 sample, is characteristic for ductile fracture. The Ni 1 sample therefore shows the most desirable fracture mode, followed by Sn 13 sample showing a mix of brittle and ductile fracture modes. The Sn 2 sample have predominantly brittle fracture modes, and therefore shows the most undesirable fracture mode of the three samples. These results are closely related with the results for elongation.

For the Ni 1.3 specimen, a river pattern were seen. (see Fig. 44) The river pattern is a result of cleavage along specific crystallographic planes, and is

a brittle fracture mechanism.[9] The presence of this fracture mode in the microstructure, builds on the tensile result, in the way that even though the Ni 1 sample is more ductile than the other two samples, it is still a brittle material.

5.2.4 EDS

The EDS results give quantitative results regarding the composition and the distribution of the different phases and elements in the material. The EDS Point scans were conducted first followed by EDS Mapping based on a SEM image of the given sample. Some of the EDS Spots were placed unfortunately in areas with topography blocking out most of the x-ray signals. There were still enough points taken to receive the quantitative data.

For the Sn 2 samples both EDS Point scans showed tungsten grains of high purity in good accordance with the insolubility of copper in tungsten. Similar results were seen for the Sn 13 sample, with the copper-tin phase showing just trace amounts of tungsten present and vice versa for copper in tungsten. The Ni 1 sample distinguish itself from the other two samples by showing amounts of chromium, nickel and iron alongside both tungsten and copper. The Ni 1 sample also showed high amounts of carbon, which probably are impurities.

The EDS Mapping scans clearly shows the mutual insolubility of tungsten and copper, with the two elements covering separate parts of the microstructure. Combined the two elements cover the whole microstructure, when pores and, for the scanning, areas shaded by topography are omitted. For both the Sn 2 and the Sn 13 samples, tin is present throughout the microstructure, but in larger portions in the copper phase. The iron is similarly present throughout the microstructure, but in larger portions in the tungsten phase.

For the Ni 1 sample it is clearly that nickel is present throughout the microstructure, and quite evenly distributed as well. Iron is similarly present throughout the microstructure, but in smaller amounts than nickel. Chromium is present similarly in the microstructure, covering some areas not covered by the two main constituents. The large amount of oxygen in these areas imply the formation of chromium oxide in the microstructure. The contribution from the oxide on the mechanical properties is unknown, but is expected to contribute with increased brittleness.

5.3 Crucible material impact

The 314 stainless steel crucible used is an austenitic steel alloy [2]. The crucible have contributed with additions of Fe and Cr (and probably some Ni also) in the material as seen from the EDS results. Surplus liquid copper during infiltration have equivalently gone into the crucible material. As noted by Neikov & Domianovich [14], Cu have a detrimental influence in steels, as it primarily goes into the steel's grain boundaries. There have been reported failure of stainless steel crucibles as a result of the infiltration process, most likely due to the copper inclusions in the microstructure combined with thermal stresses during cooling.

When looking on the effects the additions of Fe and Cr have on the material, Fe is reported to contribute with increasing the sinterability of the composite [22], similarly as Ni. The Fe inclusion should therefore give increased density of infiltrated product (closer to theoretical density). Both Fe and Cr acts, as seen in the EDS mapping results, in solid solution throughout the composite, with Fe more so than Cr.

For the effect of Cr additions in the microstructure, there is in general little literature for Cr based tungsten heavy alloys. Tejado et al. [21] compared the change in mechanical properties with temperature of the two composites W-Cu and W-CuCrZr. For the latter composite, some Cr particles were found in the structure, although no evidence pointed towards Cr having a negative impact on the mechanical performance of the composite. The W-CuCrZr showed better mechanical properties all over, both at ambient temperature and at increased temperature.

The contributions from the stainless steel on the composite are, based on the literature in general beneficial. Although beneficial, since the inclusions are added through reaction with the crucible, there is low control of the amounts of alloying elements added to the infiltrated product. To get the same beneficial effects from Fe and Cr in a more controlled manner, the elements could be included in the form of separate powders, or in alloyed powder. The use of stainless steel based crucibles have not been found in other literature, whereas most authors report the use of inert alumina or silica based crucibles [15].

5.4 Recycling and recovery

The recycling and recovery of tungsten from hard metal scraps have been utilised since the 1960s, and more improved methods have been developed through the last decade. The use of secondary sources are superior compared with using primary resources, as they yield higher WO_3 content and consume less energy and chemical reagents by requiring fewer steps to process. Tungsten is a critical material and by recycling the element is kept as part of a circular economy, reducing the footprint.

Direct recycling methods are preferred, due to yielding high quality results. Only one instance of successfully recycling of W-Cu composites using the direct cycling method zinc-melt process has been reported. This method should be tested more closely specifically for W-Cu composites.

The other direct recovery method proposed by leaching tungsten with 2:1 weight ratio of FeCl_3 -to-scrap ratio. Although leaching at elevated temperature gives complete recovery of Cu, the process decreases the yield of the tungsten by introducing hydrated tungsten oxide into the microstructure.[\[19\]](#)

Most authors are referring to indirect recycling as the most applicable type of methods for recycling of W-Cu composites. The indirect recycling methods results in the formation of APT or tungstic acid, which can be further processed to create tungsten metallic powder or other tungsten compounds. The leaching with Na_2CO_3 followed by reaction with CaCl_2 to formed CaWO_4 (scheelite).

6 Conclusion

The main objective for the thesis is to enlighten whether or not tungsten-copper composites are a viable substitute for damper mass application. Based on the experimental work and analyses, the main conclusions are:

Elastic modulus for all three samples tested are too low. Sn 13 shows the lowest modulus, as expected due to the low density, Sn 2's elastic modulus lies in between, as a compromise between high tungsten content and high porosity, while Ni 1 shows the highest elastic modulus. To fulfill the requirement a larger volume fraction of tungsten of at least 58 vol% is proposed (compared to 45 vol% currently tested).

Yield strength of all three samples tested are satisfactory. For both the Sn 2 and Ni 1 samples the criteria is also fulfilled with a good margin.

The total elongation criterion is not fulfilled for any of the samples, with only one test specimen attaining it. There is a noticeable improvement for the Ni 1 sample compared with the Sn 2 and Sn 13 samples.

The direct recycling methods are the most beneficial for both environment and economy, with low chemical consumption, but are limited to which type of scraps to be recycled. With only few claims of successful recycling of W-Cu composites for the direct methods, one should therefore focus on the indirect methods. The proposed recycling method is by leaching in Na_2CO_3 followed by adding CaCl_2 . The indirect methods can treat most tungsten scrap, but are expensive with high chemical consumption, so need to be further looked upon in an economic perspective.

The conclusion is that tungsten-copper composites show good potential to be used for the given component for dampening systems. Some alterations to the material composition are needed to fulfill all the requirements along with improved infiltration, but the NyDeMA project are on the right path towards accomplishing the aim. The material fulfill the environmental considerations, and have the potential to be a viable substitute for the material for damper mass used in dampening systems.

7 Further work

The main experimental tests not executed, due to limited lab access, were analyses of polished samples in SEM with EDS and/or Electron Backscatter Diffraction (EBSD) scan. The analyses on polished samples gives more accurate results for the composition analyses, were in the experimental work conducted fracture surface were analysed. The topography in the fracture surface lowers the output of x-rays detected, due to blocking out parts of the signal emitted from the surface atoms. A polished, flat sample is also required to be able to confidently verify the presence of intermetallic phases (IMPs). As seen in section 4.7, the high magnification images show the potential formation of IMPs in between tungsten grains for the Ni 1 sample. Analyses of polished samples could be used to verify their existence.

The nature of the possible IMPs and their effect on the mechanical properties of the composite could be further looked into. By comparing the mechanical properties of different W-Cu-Ni composites, produced by different infiltration parameters, the IMPs can be deemed having a desirable or undesirable contribution. The infiltration parameters can then be tailored to enhance the formation or prevent the growth of the IMPs, depending on the outcome.

The CT scan data can be analysed using imaging software to measure the amount of pores in the material. This way it is possible to get a more in depth look at how successful the infiltration processes have been. The results can be used in combination with the density results to give a deeper understanding of the relative density of the composite. The density results gives the average density for the whole piece measured, while the CT scan results can show how the density vary throughout the piece on a microscopic level. This way the CT scan results could give insight in geometrical limitations of the infiltrated product.

8 References

References

- [1] A. Abu-Oqail, M. Ghanim, M. El-Sheikh, and A. El-Nikhaily. “Effects of processing parameters of tungsten–copper composites”. In: *International Journal of Refractory Metals and Hard Materials* 35 (2012), pp. 207–212. ISSN: 0263-4368. DOI: <https://doi.org/10.1016/j.ijrmhm.2012.02.015>. URL: <http://www.sciencedirect.com/science/article/pii/S0263436812000364>.
- [2] H.K.D.H. Bhadesia and R.W.K. Honeycombe. *STEELS Microstructure and Properties*. Vol. 4th ed. Elsevier Ltd., 2017. Chap. 12. ISBN: 978-0-08-100270-4.
- [3] A.G. Blackman, L.R. Gahan, G. Aylward, and T. Findlay. *Aylward and Findlay’s SI chemical data*. Vol. 7th ed. John Wiley Sons Australia, Ltd, 2014. Chap. 3. ISBN: 9780730302469.
- [4] W. Callister and D. Rethwisch. *Materials Science and Engineering SI Version*. Vol. 9th ed. Wiley, 2015. Chap. 4, 8, 13, 16. ISBN: 978-1-118-31922-2.
- [5] R. Cury, J.-M. Joubert, S. Tusseau-Nenez, E. Leroy, and A. Allavena-Valette. “On the existence and the crystal structure of Ni₄W, NiW and NiW₂ compounds”. In: *Intermetallics* 17.3 (2009), pp. 174–178. ISSN: 0966-9795. DOI: <https://doi.org/10.1016/j.intermet.2008.11.001>. URL: <http://www.sciencedirect.com/science/article/pii/S0966979508002318>.
- [6] Jiten Das, A. Chakraborty, T.P. Bagchi, and Bijoy Sarma. “Improvement of machinability of tungsten by copper infiltration technique”. In: *International Journal of Refractory Metals and Hard Materials* 26.6 (2008), pp. 530–539. ISSN: 0263-4368. DOI: <https://doi.org/10.1016/j.ijrmhm.2007.12.005>. URL: <http://www.sciencedirect.com/science/article/pii/S026343680800005X>.
- [7] A. Ghaderi Hamidi, H. Arabi, and S. Rastegari. “Tungsten–copper composite production by activated sintering and infiltration”. In: *International Journal of Refractory Metals and Hard Materials* 29.4 (2011), pp. 538–541. ISSN: 0263-4368. DOI: <https://doi.org/10.1016/j.ijrmhm.2011.03.009>. URL: <http://www.sciencedirect.com/science/article/pii/S0263436811000606>.
- [8] Sarah M. Hayes and Erin A. McCullough. “Critical minerals: A review of elemental trends in comprehensive criticality studies”. In: *Resources*

- Policy* 59 (2018). Sustainable management and exploitation of extractive waste: towards a more efficient resource preservation and waste recycling, pp. 192–199. ISSN: 0301-4207. DOI: <https://doi.org/10.1016/j.resourpol.2018.06.015>. URL: <http://www.sciencedirect.com/science/article/pii/S0301420718301296>.
- [9] J. Hjelen. *Scanning elektron-mikroskopi*. SINTEF, Avdeling for metallurgi Metallurgisk institutt, NTH, Oct. 1986.
- [10] Hafed Ibrahim, Azizan Aziz, and Azmi Rahmat. “Enhanced liquid-phase sintering of W–Cu composites by liquid infiltration”. In: *International Journal of Refractory Metals and Hard Materials* 43 (2014), pp. 222–226. ISSN: 0263-4368. DOI: <https://doi.org/10.1016/j.ijrmhm.2013.12.004>. URL: <http://www.sciencedirect.com/science/article/pii/S0263436813002564>.
- [11] M. Komatani. 2014. URL: <http://www.kohsei.co.jp/english/business/kitakyushu.html>.
- [12] Nils Olav J. Meland. *Infiltration of W-Cu composites - developing a high-density material suitable for dampening systems*. Project report in TMT4500. Department of Materials Science, Engineering, NTNU – Norwegian University of Science, and Technology, Jan. 2020.
- [13] ESPI Metals. *Understanding Mesh Sizes*. URL: <https://www.espimetals.com/index.php/faq/327-technical-data/stainless-steel/334-%20understanding-mesh-sizes>.
- [14] Oleg Domianovich Neïkov. *Handbook of Non-Ferrous Metal Powders : Technologies and Applications*. Vol. 1st ed. Elsevier Science, 2009. Chap. 21. ISBN: 9781856174220. URL: <http://search.ebscohost.com/login.aspx?direct=true&db=e230xww&AN=249334&site=ehost-live>.
- [15] G. Prabhu, N. Arvind Kumar, M. Sankaranarayana, and T.K. Nandy. “Tensile and impact properties of microwave sintered tungsten heavy alloys”. In: *Materials Science and Engineering: A* 607 (2014), pp. 63–70. ISSN: 0921-5093. DOI: <https://doi.org/10.1016/j.msea.2014.03.130>. URL: <http://www.sciencedirect.com/science/article/pii/S0921509314004237>.
- [16] A. Shemi, A. Magumise, S. Ndlovu, and N. Sacks. “Recycling of tungsten carbide scrap metal: A review of recycling methods and future prospects”. In: *Minerals Engineering* 122 (2018), pp. 195–205. ISSN: 0892-6875. DOI: <https://doi.org/10.1016/j.mineng.2018.03.036>. URL: <http://www.sciencedirect.com/science/article/pii/S0892687518301432>.
- [17] Leiting Shen, Xiaobin Li, Daniel Lindberg, and Pekka Taskinen. “Tungsten extractive metallurgy: A review of processes and their challenges

- for sustainability”. In: *Minerals Engineering* 142 (2019), p. 105934. ISSN: 0892-6875. DOI: <https://doi.org/10.1016/j.mineng.2019.105934>. URL: <http://www.sciencedirect.com/science/article/pii/S0892687519303450>.
- [18] J.K. Solberg. *TEKNOLOGISKE METALLER OG LEGERINGER*. NTNU, Institutt for materialteknologi, 2014. Chap. 4, 5.
- [19] R.R. Srivastava, J. Lee, M. Bae, and V. Kumar. “Reclamation of tungsten from carbide scraps and spent materials”. In: *J Mater Sci* 54 (2019), pp. 83–107. DOI: <https://doi.org/10.1007/s10853-018-2876-1>. URL: <https://link.springer.com/article/10.1007/s10853-018-2876-1>.
- [20] Shuang Su and Yunzhuo Lu. “Densified WCu composite fabricated via laser additive manufacturing”. In: *International Journal of Refractory Metals and Hard Materials* 87 (2020), p. 105122. ISSN: 0263-4368. DOI: <https://doi.org/10.1016/j.ijrmhm.2019.105122>. URL: <http://www.sciencedirect.com/science/article/pii/S0263436819305773>.
- [21] E. Tejado, A.V. Müller, J.H. You, and J.Y. Pastor. “Evolution of mechanical performance with temperature of W/Cu and W/CuCrZr composites for fusion heat sink applications”. In: *Materials Science and Engineering: A* 712 (2018), pp. 738–746. ISSN: 0921-5093. DOI: <https://doi.org/10.1016/j.msea.2017.12.054>. URL: <http://www.sciencedirect.com/science/article/pii/S0921509317316520>.
- [22] Ning Zhang, Zhe Wang, Lei Guo, Long Meng, and Zhancheng Guo. “Rapid fabrication of W–Cu composites via low-temperature infiltration in supergravity fields”. In: *Journal of Alloys and Compounds* 809 (2019), p. 151782. ISSN: 0925-8388. DOI: <https://doi.org/10.1016/j.jallcom.2019.151782>. URL: <http://www.sciencedirect.com/science/article/pii/S0925838819330154>.
- [23] K. Zhou, W.G. Chen, J.J. Wang, G.J. Yan, and Y.Q. Fu. “W–Cu composites reinforced by copper coated graphene prepared using infiltration sintering and spark plasma sintering: A comparative study”. In: *International Journal of Refractory Metals and Hard Materials* 82 (2019), pp. 91–99. ISSN: 0263-4368. DOI: <https://doi.org/10.1016/j.ijrmhm.2019.03.026>. URL: <http://www.sciencedirect.com/science/article/pii/S0263436819301751>.

Appendix

A Computerized Tomography (CT)

Images through the fracture area were assembled into videos, which can be assessed by following this link: <https://www.youtube.com/playlist?list=PLTGhGkqbn5LPiG97Ic0eujlQLYmBiigXl> The videos show the variation in the topography through the fracture area, with the Ni 1 sample having the largest change in the topography. A large change in topography in the fracture area is in accordance with a ductile fracture, opposed to a brittle fracture which gives flat fracture surfaces. The test therefore highlights the Ni 1 sample to be more ductile than the other two samples.

